Atomic layer deposition of silicon-based dielectrics for semiconductor manufacturing: Current status and future outlook

Rafaiel A. Ovanesyan, Ekaterina A. Filatova, Simon D. Elliott, Dennis M. Hausmann, David C. Smith, and Sumit Agarwal

Citation: Journal of Vacuum Science & Technology A **37**, 060904 (2019); doi: 10.1116/1.5113631
View online: https://doi.org/10.1116/1.5113631
View Table of Contents: https://avs.scitation.org/toc/jva/37/6
Published by the American Vacuum Society

Atomic layer deposition of silicon-based dielectrics for semiconductor manufacturing: Current status and future outlook

Rafaiel A. Ovanesyan,[1] Ekaterina A. Filatova,[2] Simon D. Elliott,[3] Dennis M. Hausmann,[4] David C. Smith,[4] and Sumit Agarwal[1]
[1]*Department of Chemical and Biological Engineering, Colorado School of Mines, Golden, Colorado 80401*
[2]*Tyndall National Institute, University College Cork, Cork T12 R5CP, Ireland*
[3]*Schrödinger Inc., 120 West 45th Street, New York, New York 10036*
[4]*Lam Research Corporation, Tualatin, Oregon 97062*

(Received 11 June 2019; accepted 22 August 2019; published 24 September 2019)

The fabrication of next-generation semiconductor devices has created a need for low-temperature (≤400 °C) deposition of highly-conformal (>95%) SiO_2, SiN_x, and SiC films on high-aspect-ratio nanostructures. To enable the growth of these Si-based dielectric films, semiconductor manufacturers are transitioning from chemical vapor deposition to atomic layer deposition (ALD). Currently, SiO_2 films deposited using ALD are already being integrated into semiconductor device manufacturing. However, substantial processing challenges remain for the complete integration of SiN_x films deposited by ALD, and there are no known processes for ALD of SiC at temperatures that are compatible with semiconductor device manufacturing. In this focused review, the authors look at the status of thermal and plasma-assisted ALD of these three Si-based dielectric films. For SiO_2 ALD, since low-temperature processes that deposit high-quality films are known, the authors focus primarily on the identification of surface reaction mechanisms using chlorosilane and aminosilane precursors, as this provides a foundation for the ALD of SiN_x and SiC, two material systems where substantial processing challenges still exist. Using an understanding of the surface reaction mechanisms, the authors describe the underlying reasons for the processing challenges during ALD of SiN_x and SiC and suggest methodologies for process improvement. While both thermal and plasma-assisted SiN_x ALD processes have been reported in the literature, the thermal NH_3-based ALD processes require processing temperatures >500 °C and large NH_3 doses. On the other hand, plasma-assisted SiN_x ALD processes suffer from nonuniform film properties or low conformality when deposited on high-aspect-ratio nanostructures. In the SiN_x section, the authors provide a broad overview of the currently known thermal and plasma-assisted SiN_x ALD processes using chlorosilane, trisilylamine, and aminosilane precursors, describe the process shortcomings, and review the literature on precursor reaction pathways. The authors close this section with suggestions for improving the film properties and conformality. In the case of SiC, the authors first outline the limitations of previously reported SiC ALD processes and highlight that unlike SiO_2 and SiN_x plasma-assisted ALD, no straightforward pathway for low-temperature plasma-assisted growth is currently apparent. The authors speculate that low-temperature ALD of SiC may require the design of completely new precursors. Finally, they summarize the progress made in the ALD of C-containing SiN_x and SiO_2 films, which may provide many of the benefits of SiC ALD in semiconductor manufacturing. In closing, through this review, the authors hope to provide the readers with a comprehensive knowledge of the surface reactions mechanisms during ALD of Si-based dielectrics, which would provide a foundation for future precursor and process development.
https://doi.org/10.1116/1.5113631

I. INTRODUCTION

The miniaturization of microelectronic devices has introduced several processing challenges that need to be overcome for the implementation of advanced architectures at sub-7-nm technology nodes.[1,2] In particular, the introduction of FinFET-based transistor devices and the rapid proliferation of 3D NAND memory have created a need for thin film growth processes capable of depositing materials with a conformality of >95% at temperatures ≤400 °C over high aspect ratio (HAR) nanostructures.[3] In the semiconductor industry, two of the most commonly used thin film growth techniques are thermal chemical vapor deposition (CVD) and plasma-assisted CVD. While thermal CVD does provide a limited capability for conformal film growth,[4,5] the deposition temperature at which growth occurs is often too high,[6] which makes it unsuitable for applications with a limited thermal budget. On the other hand, plasma-assisted CVD allows for the growth of high-quality films at substrate

Note: This paper is part of the 2020 Special Topic Collection on Atomic Layer Deposition (ALD).

temperatures lower than thermally driven CVD processes, and within the typical thermal budget for semiconductor manufacturing,[7–9] but growth is typically nonconformal due to line of sight deposition from very reactive radicals that are produced in the plasma environment.[10] As the critical dimensions of semiconductor devices continue to shrink,[11] plasma-assisted CVD processes become more difficult to integrate due to the possibility of pinch-off in HAR structures. Therefore, to mitigate the shortcomings of CVD processes, and to enable the growth of highly-conformal films at low substrate temperatures, semiconductor manufacturers are turning to atomic layer deposition (ALD) as a potential alternative.

ALD is a thin film growth technique that has found broad application in a variety of areas including microelectronics, solar cells, and optical devices.[3] ALD is similar to CVD, but distinct in the sense that the deposition process is split into half-reactions. ALD is characterized by the exposure of a substrate to a repeating series of two or more alternating precursor doses separated by an inert purge. Crucially, the individual precursor chemicals react initially with the growing surface and then do not react any further, limited by the surface itself,[3,12] which leads to self-limiting growth and allows for the deposition of highly-conformal, ultrathin films at a typical growth per cycle (GPC) on the orderer of 1 Å.[3,12] ALD processes come in two types, thermal and plasma-assisted. In a thermal ALD process, the activation of the surface reactions that lead to film growth is achieved by the temperature of the substrate.[13] In contrast, in plasma-assisted ALD processes, radicals and ions generated in the plasma half-cycle allow growth reactions to take place at lower temperatures and lower precursor exposure.[14] The gases that are typically used in plasma-assisted ALD are O_2 for oxide growth, N_2 or NH_3 for nitride growth, and H_2 for metal growth, as plasmas of these gases lead to self-limiting surface reactions. In contrast, plasmas of gases such as SiH_4 and CH_4 cannot be used in plasma-assisted ALD as they lead to continuous film growth. Both thermal and plasma-assisted ALDs have been extensively reviewed.[3,12,13,15–19] This review will focus on the ALD of Si-based dielectrics—their applications in semiconductor manufacturing, the film growth mechanisms and how these in turn influence the film properties, and finally identify areas for further research and development.

A. Applications of ALD of Si-based dielectrics in the semiconductor industry

ALD became prominent in semiconductor manufacturing for the deposition of high-permittivity (κ) oxide materials. For instance, HfO_2 deposited by ALD was used to replace thermally-grown SiO_2 as the gate dielectric material in traditional metal oxide semiconductor field effect transistors.[3,20] More recently, there has been substantial growth in the number of applications that require the use of ALD.[3] It is needed in microelectronics for applications such as the encapsulation of gate stacks and advanced memory structures, including magnetoresistive random-access memory (RAM) and phase-change RAM.[21] For these applications, ALD is needed due to the conformality requirements and the pitch of the device structure.[21] Of the many materials that can be deposited via ALD, Si-based dielectric materials are used in certain key applications discussed later in this section. Therefore, in this review, we focus on the ALD of the Si-based dielectrics SiO_2, SiN_x, and SiC that are currently the most important to the semiconductor industry (see Fig. 1).[22–25] The ALD of these three Si-based currently dielectrics represents a substantial segment of the ALD market and will continue to be crucial for the creation of advanced electronic devices in the near future.[24] These three Si-based dielectrics have different optical, electronic, and barrier properties, as well as different etch selectivities relative to one another, making them suitable for a wide variety of applications. Furthermore, these materials are essential building blocks for several ternary blends, such as silicon carbon oxide (SiCO), silicon carbon nitride (SiCN), and silicon oxynitride (SiON), which also have unique applications in semiconductor manufacturing, and are also described below.

In the semiconductor industry, ALD of SiO_2 has applications such as sidewall spacers,[26] shallow trench isolation liners,[27] and gate stack liners.[11] The ALD of SiN_x can be used for fabricating sidewall spacers,[10,28] trench liners, gate stack encapsulation,[28] and air gap liners.[29] SiC is often used as a hard mask layer because of its robust resistance to chemical and plasma etching.[30] SiCO can be used for similar applications as SiO_2, but also finds application as a low-κ dielectric for interconnects.[31,32] Materials with a low dielectric constant have been discussed in detail by several authors.[31,33] Similarly, SiCN can be used in applications typically reserved for SiN_x but has the added benefit of a lower dielectric constant.[31,33] These low-κ materials can improve the performance of semiconductor devices by reducing resistive-capacitive delays.[31,33] Furthermore, SiCN is used as an etch-stop layer,[34] while SiON has been used as an antireflection coating.[35] The numerous potential applications for Si-based dielectrics make this class of materials extremely important to the semiconductor industry. Herein, we limit the discussion to three applications of ALD in the semiconductor industry: the formation of sidewall spacers in self-aligned

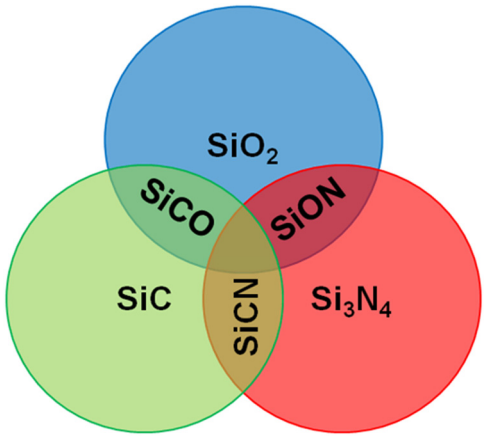

FIG. 1. Diagram showing the three most technologically relevant Si-based dielectrics and their ternary blends.

multiple patterning (SAxP),[36] metal word line formation in 3D NAND memory,[37] and the formation of sidewall spacers in FinFET structures.[26]

SAxP was introduced into semiconductor manufacturing to overcome current limitations of optical lithography based on a 193 nm ultraviolet source, which has a resolution limit of ~40 nm.[36,38] SAxP uses sacrificial mandrels that are created using traditional optical lithography and that are then conformally coated with a thin film whose planar surfaces are subsequently removed through dry etching to form sidewall spacers as shown in Fig. 2(a).[39,40] This film is typically deposited using ALD because the thickness and material properties of the deposited films must be similar on both the planar and sidewall surfaces.[38] The mandrels are then removed, leaving behind only the sidewall spacers. Afterwards, the underlying substrate is etched, and the remaining sidewall spacers are removed to create structures smaller than those allowed by traditional 193 nm optical lithography. Furthermore, because there are two sidewall spacers per sacrificial mandrel, SAxP can effectively double the pattern density. If the SAxP process is repeated twice, it leads to a quadrupling of the pattern density.[41]

The fabrication of 3D NAND memory devices has also greatly benefited from the introduction of ALD, where it has enabled the manufacturing of ultradense memory [see Fig. 2(b)].[42] ALD is used to deposit a dielectric film on the sidewalls of the HAR holes connecting the numerous layers of the 3D NAND memory structure, as well as for the deposition of metal in the horizontally oriented HAR word lines.[42] ALD is preferred because of the extremely narrow HAR geometry present in 3D NAND memory devices.[42] In 3D FinFET structures, which were introduced to improve transistor performance and increase packing density by shrinking the critical dimensions, one of the applications of ALD is for the formation of ultrathin sidewall spacers that electronically isolate the gate stack from the HAR fin structures [see Fig. 2(c)].[43]

B. Characterization of chemical mechanisms

Despite the need for the ALD of Si-based dielectrics in the semiconductor industry, the development of ALD processes that are capable of depositing high-quality, conformal, Si-based dielectric films at low substrate temperatures has proven to be challenging with SiO_2 and SiN_x at different stages of integration into manufacturing. In the case of SiO_2, there are several ALD processes capable of depositing high-quality SiO_2 films within the required processing parameters. For the ALD of SiN_x, while low-temperature ALD processes are known, there are still processing challenges, such as poor film quality or low conformality, that must be addressed. In the case of SiC ALD, no known low-temperature ALD processes exist.

To understand, and potentially overcome the remaining challenges associated with the ALD of Si-based dielectrics, one approach is to look at the ALD half-reactions from a mechanistic perspective.[44] The first level of mechanistic understanding is writing balanced chemical equations for the overall process and for each precursor half-cycle, listing the main by-products and showing the nature of the saturating surfaces. A deeper level of mechanistic understanding concerns the nature of each elementary step of the chemical reaction.[45–57] The primary reaction steps in each ALD cycle may include (i) molecular physisorption of the precursor onto a suitably-prepared surface, (ii) molecular or dissociative chemisorption, (iii) local transfer of ligands and/or fragments between precursor and surface, (iv) longer-scale diffusion and reorganization, and (v) desorption of by-products.[44] Under ideal ALD conditions, the net adsorption of new material self-limits in both of the ALD pulses, despite the presence of the excess gas-phase precursor. Under more realistic ALD conditions, these reactions are in competition with non-ALD reactions that do not self-limit, such as gas-phase thermolysis, surface-catalyzed ligand decomposition, and impurity incorporation. In plasma-assisted ALD, one of the half-cycles is replaced with a plasma step. In some of these processes, the reactions in the nonplasma half-cycle are similar to those in the completely thermal ALD process. In fact, in cases such as ALD of Al_2O_3, the surface termination following *both* half-cycles can be similar in the thermal and plasma-assisted processes.[54,58,59] However, a key difficulty in plasma-assisted ALD processes is the identification of the reactive species within the plasma that are responsible for film growth. Additional effects, such as redeposition of removed surface species[60] and ion-induced surface modification,[61,62] may also be present in plasma-assisted ALD.

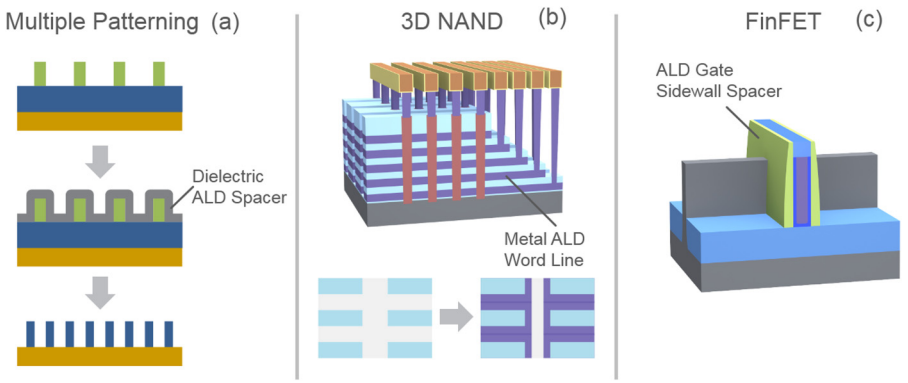

FIG. 2. Applications of ALD in semiconductor device manufacturing.

The half-reactions during ALD have primarily been investigated using *in situ* surface characterization techniques such as Fourier transform infrared (FTIR) spectroscopy and by first principles calculations, usually density functional theory (DFT). *In situ* infrared spectroscopy is a powerful technique in the study of surface reactions during the ALD of Si-based dielectrics as it allows for the direct observation of the Si—N—Si, Si—O—Si, and Si—C—Si phonon modes, as well as the vibrational modes associated with —SiH_x ($x = 1$, 2, or 3), —NH_x ($x = 1$ or 2), —CH_x ($x = 1$, 2, or 3), —$SiCl_x$ ($x = 1$, 2, or 3), and —OH, which are the most common surface functional groups during the ALD of Si-based dielectrics.[47,63] Surface infrared spectroscopy has been described in detail in previous publications.[47–49] *In situ* FTIR spectroscopy can be sensitive enough to probe even submonolayer surface coverages, allowing for the direct observation of the changes on the surface following each precursor half-cycle during the ALD process.[64] Surface reaction mechanisms have been studied primarily using two FTIR spectroscopy techniques: transmission and attenuated total reflection (ATR) FTIR spectroscopy. Transmission FTIR spectroscopy uses a deposition substrate such as an Si wafer or a pelletized infrared transparent powder such as KBr or ZrO_2: the powder approach is used to obtain a high surface area to enhance sensitivity. On the other hand, ATR-FTIR spectroscopy uses an internal reflection element as the deposition substrate and relies on multiple internal reflections to enhance sensitivity to monitor even submonolayer surface coverages rapidly.[64,65] Using FTIR spectroscopy, it is possible to monitor the film composition, reactive surface sites, and adsorbed surface species during each precursor half-cycle and therefore identify the surface reaction mechanisms.[64]

In addition to *in situ* surface characterization, first principles DFT calculations can be used to calculate the energetics of the surface reactions during precursor cycles, which reveals the chemical mechanism and allows for rapid precursor screening.[44,66,67] Mechanistic knowledge can then inform substrate preparation, reactor conditions, and choice of chemicals. Choosing the right precursor for an ALD process is a crucial factor in determining the viability of the process and the quality of the grown film, and this is greatly aided by understanding the ALD chemistry. Detailed knowledge of the reaction steps can help in the selection of chemistry that minimizes activation energies for the ALD reactions and avoids unwanted side reactions, enabling low-temperature ALD of pure materials.

In this review article, we discuss the current status of the ALD of SiO_2, SiN_x, and SiC. In particular, we describe the advantages and limitations of the known thermal and plasma-assisted ALD processes, and whenever possible, identify the surface reaction mechanisms that lead to film growth, and discuss how the surface reaction mechanisms influence film properties. Finally, we identify the remaining challenges for the ALD of Si-based dielectrics and describe the progress made in the ALD of ternary blends.

This review is structured as follows. In Sec. II, we describe the ALD of SiO_2, with a particular focus on the surface reaction mechanisms that lead to film growth for chlorosilane, Si alkoxide, and aminosilane Si precursors. In Sec. III, we outline the challenges for both thermal and plasma-assisted SiN_x ALD processes, namely, those using chlorosilanes, trisilylamine (TSA), or aminosilanes, as the Si precursor. We then identify the surface reaction mechanisms and describe the computational studies on precursor reactivity. Finally, in Sec. IV, we outline the challenges associated with the ALD of SiC and summarize the progress made toward C incorporation during the ALD of SiO_2 and SiN_x films.

II. ATOMIC LAYER DEPOSITION OF SiO_2

SiO_2 ALD has been widely studied over the last two decades. Figure 3 shows a scanning electron microscopy image of an SiO_2 film deposited by ALD with a conformality of >95%, which clearly demonstrates that current ALD processes can provide the attributes required for semiconductor manufacturing. As the breadth of the literature on SiO_2 ALD is extensive, we limit this review to the most industrially-relevant SiO_2 ALD processes. A recent comprehensive review of precursors used in ALD of SiO_2 was carried out by Miikkulainen *et al.*[15] Progress in theoretical modeling of SiO_2 ALD was recently reviewed in detail by Fang *et al.*[68]

Silane is the most common Si precursor for thin film growth of Si-based materials for semiconductor manufacturing. However, SiH_4 is not a suitable precursor for the ALD of SiO_2 due to very weak molecular adsorption on a hydroxylated SiO_2 surface, and a very high barrier toward subsequent hydride elimination.[69] Alkylsilanes, another common set of precursors in thermal and plasma-assisted CVD of Si-based materials, are similarly unreactive at temperatures relevant for ALD.[48] Therefore, to enable the ALD of SiO_2, more reactive Si precursors are required. In this section, we primarily review the chemical mechanisms of SiO_2 ALD using chlorosilane, Si alkoxide, and aminosilane precursors with typical oxygen-containing precursors such as H_2O, O_2 plasma, or O_3.

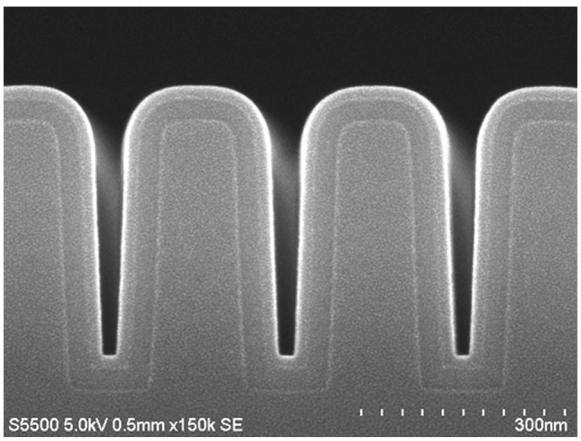

FIG. 3. Scanning electron microscopy image of an SiO_2 film deposited using a bis(*tert*-butylamino)silane ($SiH_2(NH^tBu)_2$, BTBAS) and O_2 plasma ALD process at 400 °C on a nanostructure with an aspect ratio of ~4.5.

A. Chlorosilanes

In one of the first reports on SiO_2 ALD, Sneh *et al.*[70] demonstrated the ALD of SiO_2 using $SiCl_4$ and H_2O. The processing temperature was >327 °C, but required large $SiCl_4$ exposures (>10^9 L). This is consistent with prior work reported by Tripp and Hair on the functionalization of —OH-terminated SiO_2 surfaces, where these authors reported temperatures >300 °C for reaction of alkylated chlorosilanes with hydroxylated SiO_2.[71–74] The reaction cycle for SiO_2 ALD from $SiCl_4$ and H_2O is illustrated in Fig. 4. The change in bond energies during both half-reactions indicates that both steps should be moderately exothermic. The reason for the high processing temperature and large $SiCl_4$ doses lies in the kinetics of the reactions. Sneh *et al.* proposed that, in the $SiCl_4$ half-cycle, the precursor initially physisorbs via H-bonding on hydroxylated SiO_2, rather than undergoing dissociative chemisorption [see Fig. 5(a)]. The subsequent reaction is direct substitution, i.e., concurrent cleavage of Si—Cl and O—H occurs with the formation of Si—O and H—Cl via a four-membered-ring transition state (TS) where the Si atom in $SiCl_4$ is fivefold coordinated [see Fig. 5(b)]. The result is chemical bonding of the chlorosilane fragment to the surface via the surface O atom, and the formation of HCl as a by-product. The rate of the substitution reaction thus depends in part on the strength of molecular adsorption and the geometry of that intermediate. The authors suggested that a similar mechanism may be at play during the H_2O half-cycle [see Figs. 5(c) and 5(d)].

DFT calculations by Kang and Musgrave on hydroxylated Si(100) provided further evidence that individual molecules indeed adsorb and eliminate HCl in one step via a single four-membered-ring TS in both the $SiCl_4$ and H_2O half-cycles.[75] However, in a later DFT study of ALD of SiO_2 onto hydroxylated α-SiO_2(0001), Fang *et al.*[76] reported metastable intermediates with pentacoordinate Si in both $SiCl_4$ and H_2O pulses. This conflicting evidence suggests that the local environment has a major influence on whether pentacoordinate Si is metastable or unstable.

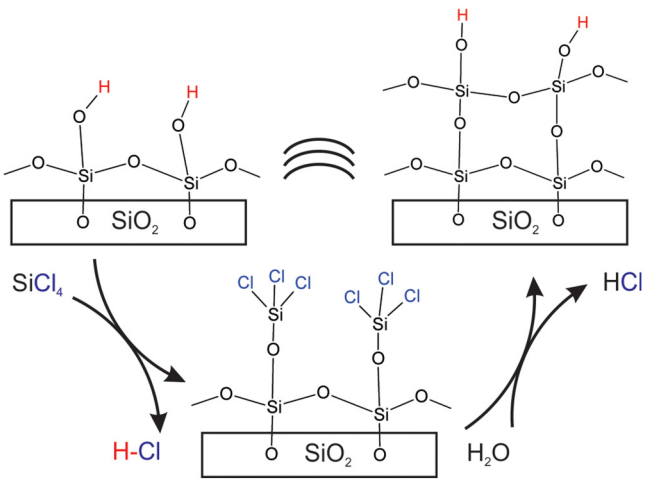

FIG. 4. Schematic ALD cycle at steady state for SiO_2 from pulses of $SiCl_4$ and H_2O.

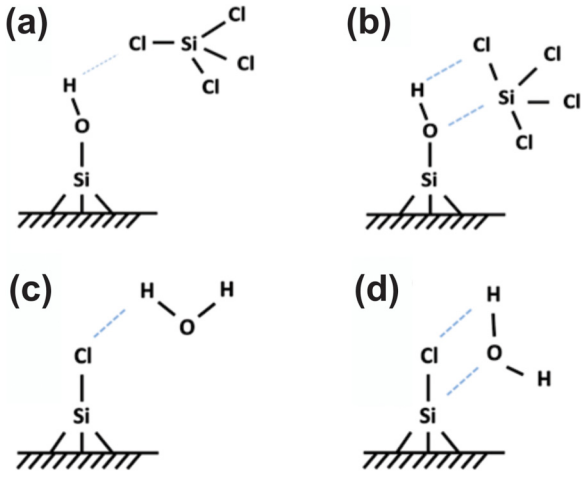

FIG. 5. SiO_2 ALD mechanism during $SiCl_4$ and H_2O pulses. $SiCl_4$ precursor physisorbs on hydroxylated silica via H-bonding followed by direct substitution, i.e., concurrent cleavage of Si—Cl and O—H and formation of Si—O and H—Cl via a four-membered-ring transition state with pentacoordinate Si. H_2O physisorbs on surface Si—Cl via H-bonding followed by direct substitution, i.e., concurrent cleavage of Si—Cl and O—H and formation of Si—O and H—Cl via a four-membered-ring TS.

Sneh *et al.* also verified the surface reaction mechanism for SiO_2 ALD from $SiCl_4$ and H_2O using transmission FTIR spectroscopy (see Fig. 6).[70] Figure 6 shows the infrared difference spectra for the $SiCl_4$ and H_2O half-reactions. As can be seen in Fig. 6, the starting surface for the $SiCl_4$ half-cycle is populated by isolated Si—OH species as evidenced by the presence of the —OH stretching vibration at ~3750 cm^{-1}. Following exposure to $SiCl_4$, the isolated —SiOH species are removed and an —$SiCl_x$ ($x = 1, 2, 3$) terminated surface is created, as shown by the increase in the —$SiCl_x$ ($x = 1, 2, 3$) stretching mode at ~650 cm^{-1}, and a decrease in absorbance in the —OH stretching region. During the H_2O half-cycle, the —$SiCl_x$ ($x = 1, 2, 3$) species are removed and the —SiOH terminated surface is recreated, allowing for the continuation of the ALD process.

The reaction temperature and precursor exposure time for SiO_2 ALD from chlorosilanes and H_2O can be lowered using a nucleophilic molecule as a catalyst. Tripp and Hair first reported this effect in 1993 using multiple cycles of alternating alkylchlorosilane and H_2O pulses catalyzed with amines.[71] However, they did not describe this as ALD. Exposure to triethylamine allowed the surface reaction to proceed at room temperature. This is consistent with the mechanism proposed by Blitz *et al.*[77] whereby H-bonding of an amine base to surface hydroxyl increases the nucleophilicity (i.e., electron donating power) of oxygen in the hydroxyl group, facilitating chemisorption of chlorosilane via pentacoordinate Si (see Fig. 7). Importantly, this pentacoordinate structure was proposed to be a metastable intermediate, rather than a transient TS.[77] In molecular chemistry, pentacoordinate Si is known to be stable when bonded to highly electronegative atoms such as F, Cl, or O (i.e., hard bases).

George and co-workers also studied base-catalyzed thermal ALD of SiO_2 from $SiCl_4$ and H_2O (Ref. 78) and confirmed that codosing with pyridine in each half-cycle

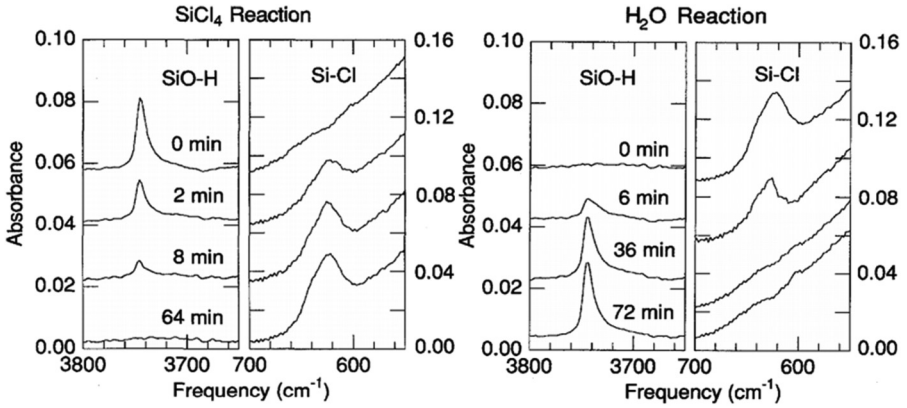

FIG. 6. Infrared transmission spectra for the H_2O and $SiCl_4$ half-cycles during SiO_2 ALD at 327 °C. The Si—OH and the —$SiCl_x$ ($x = 1, 2, 3$) stretching region are shown. Reproduced with permission from Sneh *et al.*, Surf. Sci. **334**, 135 (1995) (Ref. 70). Copyright 1995 Elsevier.

permitted lower temperatures (25 °C) and smaller precursor doses (10^4 l). The H_2O half reaction was found to saturate faster than the $SiCl_4$ half reaction, implying that the latter is rate-determining at low temperatures. Fitting first order kinetics to the data revealed that the effective activation energy was halved by base-catalysis, and this dramatic drop in activation energy was later confirmed in DFT models by Chen *et al.*[79] It appears that OH or H_2O is activated by an intermediate with H-bonded pyridine and pentacoordinate Si, as proposed by Blitz *et al.*[77] (see Fig. 7). The George group used transmission FTIR to monitor the surface —SiOH and pyridine vibrations to provide evidence for these intermediates.[80] The presence of these intermediates was verified by showing that during adsorption, pyridine hydrogen bonds with the isolated —SiOH groups, which have a stretching mode at ~3750 cm^{-1}: the H-bonding can be evidenced by the decrease in the peak intensity and red-shifting the characteristic frequency. In addition, vibrational modes associated with pyridine appear in the infrared spectra, corresponding to H-bonded pyridine on the surface.[80] Chen *et al.* showed that smaller and more alkaline Lewis bases had a stronger catalytic effect during ALD of SiO_2.[79] Consistent with this, George *et al.* experimentally showed that NH_3 was ~10 times more effective as a catalyst for this reaction than pyridine, forming a less strained TS via extra protons for H-bonding and/or elimination as HCl. However, the primary drawback of using NH_3 is the formation of involatile NH_4Cl due to reaction with HCl, which can accumulate in the reactor leading to particle formation.[81] Using DFT, Fang *et al.*[76] simulated the reaction of H_2O with a Cl-terminated SiO_2 surface. These calculations also showed that the activation energies were lowered by at least a third through the coordination of a second adsorbing H_2O in an H-bonded intermediate [see Fig. 7(d)], acting as nucleophile and proton source, in the same way as NH_3. The authors also reported a low activation energy barrier for condensation reactions to form H_2O or HCl along with Si—O—Si bridges.[76]

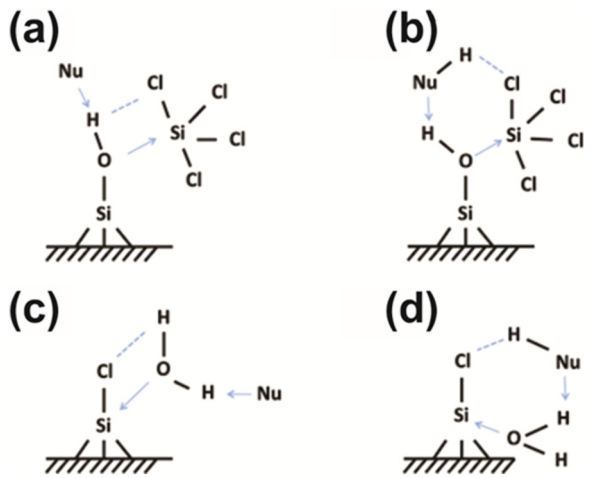

FIG. 7. Reaction mechanism of SiO_2 ALD catalyzed by amine base during the $SiCl_4$ and H_2O pulses. H-bonding of a nucleophile (Nu) such as an amine to surface —OH [(a) and (b)] or H_2O [(c) and (d)] increases the reactivity of oxygen in that group toward Si, facilitating chemisorption of the (a) chlorosilane or (c) water, both via pentacoordinate Si in a four-membered ring. A nucleophile with acidic H (NuH) allows for the formation of a more stable six-membered ring [(b) and (d)].

This sequence of studies on chlorosilanes shows how particular reagents may open up new mechanistic pathways and have a major effect on the viability of an ALD process. $SiCl_4$ cannot chemisorb molecularly and faces a high barrier toward the elimination of HCl, due to strain in the four-membered —Si—O—H—Cl— ring of the TS. Thermal ALD is then only possible above 323 °C.[71] Codosing with a nucleophilic reagent (e.g., pyridine) increases the reactivity of the surface and allows $SiCl_4$ to adsorb molecularly as the pentacoordinate intermediate —$OSiCl_4$, lowering the barrier to HCl formation.[78] The temperature where ALD is viable thus drops to 23 °C. Codosing with a protic nucleophile (e.g., NH_3) changes the TS into a six-membered ring, further accelerating the reaction.[81] H_2O is also a protic nucleophile and so the same effect makes the H-bonded network of adsorbed H_2O molecules reactive toward the Cl-terminated surface. This explains why the H_2O pulse does not require high temperatures in this process. It also explains why non-protic oxygen sources, such as O_2 or O_3, do not perform as well as thermal H_2O with $SiCl_4$.[82,83] Another obstacle in these cases is the absence of H in $SiCl_4$, meaning that oxidation cannot generate a hydroxyl-covered surface during

ALD.[84] We expect that one consequence is a lower ALD growth per cycle for these oxygen sources, because less HCl can be eliminated in the $SiCl_4$ pulse than when hydroxyl groups are present.

While base-catalyzed SiO_2 ALD processes that use $SiCl_4$ and H_2O precursors are capable of film growth at low temperatures and small precursor exposures, a chlorine-free low-temperature ALD process would be preferred for many applications, because HCl produced as a by-product is highly corrosive and undergoes further side reactions. Therefore, for semiconductor device manufacturing, other chlorine-free Si precursors such as Si alkoxides and aminosilanes are also of interest.

B. Alkoxides

As Si alkoxides are relatively unreactive, base-catalysis also seems to be key to achieving ALD of SiO_2 using alkoxide precursors. For instance, SiO_2 was grown by ALD just above room temperature using tetraethoxysilane and H_2O as precursors with NH_3 as a catalyst.[85] Infrared data indicate that NH_3 increased the nucleophilicity of oxygen in surface SiOH, possibly as shown for chlorosilanes in Fig. 7.[85] The self-catalytic precursor $H_2N(CH_2)_3Si(OEt)_3$ has also been used with H_2O or O_3 for low-temperature ALD (120–200 °C).[52,86] Similar chemistry can be expected for azasilanes that produce amino groups on ring-opening.[87] It seems likely that the amino group of the precursor both improves adsorption and increases the reactivity of surface hydroxyl groups toward the alkoxide ligands. In a similar fashion, a $(CH_3)_3Al$ catalyzed SiO_2 ALD process was reported by Hausmann *et al.*[88]

Hausmann *et al.* reported a "Rapid ALD" process for SiO_2 nanolaminates from $(Bu^tO)_3Si(OH)$ and $(CH_3)_3Al$.[88] In this mechanism, the $(CH_3)_3Al$ reacts with surface —SiOH species to form an $—OAlCH_3$ terminated surface [see Fig. 8(a)]. The Al—O bond then catalyzes the reaction of the $(Bu^tO)_3Si(OH)$ precursor with the $—OAlCH_3$ surface species to form an $—AlOSi(Bu^tO)_3$ terminated surface with CH_4 liberated into the gas phase [Fig. 8(b)]. Subsequent $(Bu^tO)_3Si(OH)$ precursor exposure leads to further catalyzed reaction, through the elimination of Bu^tOH species [Fig. 8(c)]. The continued catalyzed $(Bu^tO)_3Si(OH)$ precursor decomposition continues until ~12 nm of SiO_2 film is deposited. The proposed mechanism in Fig. 8 has been verified using DFT by Ni *et al.*[89] In this case, it appears that Al—O units can catalyze decomposition of the precursor via Lewis acid/base interaction, yielding siloxane oligomers that cross-link to SiO_2. This is, therefore, another case of the catalytic activation of —SiOH, albeit via a Lewis adduct rather than via H-bonding.

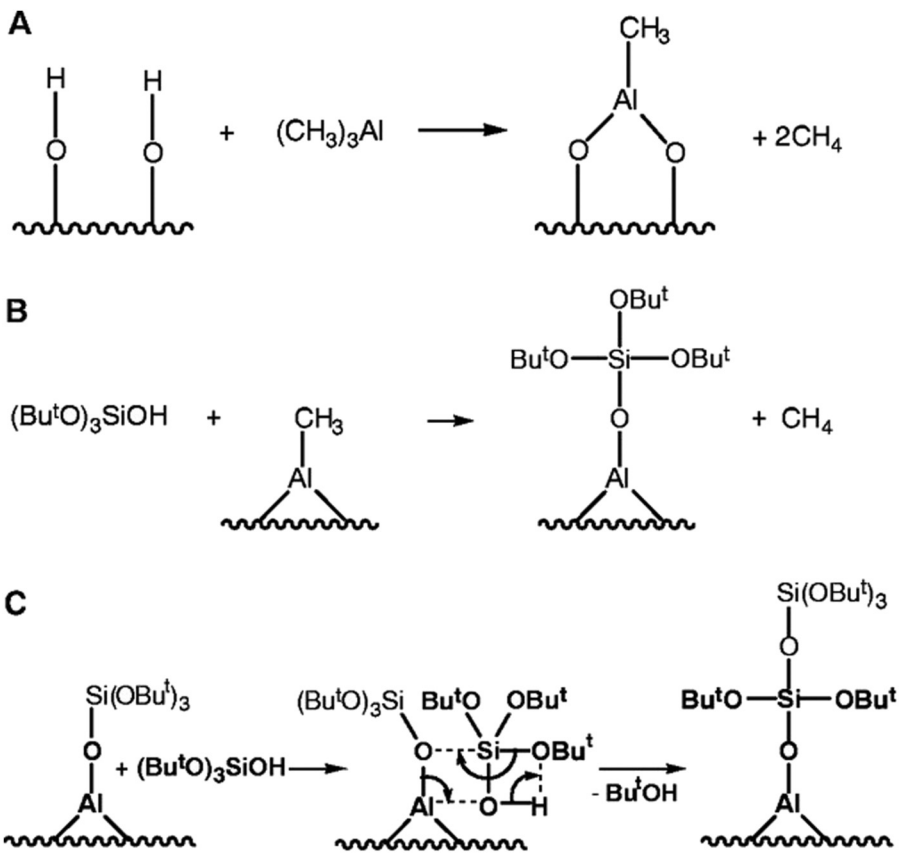

FIG. 8. Cooperative effect of $(CH_3)_3Al$ in SiO_2 nanolaminate ALD. Initially, (a) the $(CH_3)_3Al$ reacts with surface —SiOH species to form an $—O_2AlCH_3$ terminated surface through the elimination of two CH_4 molecules. The presence of the Al—O bond catalyzes the reaction of $(Bu^tO)_3SiOH$ with the $—O_2AlCH_3$ terminated surface via the formation of $—AlOSi(Bu^tO)_3$ surface species with CH_4 as the gaseous by-product (b). The Al—O bonds further catalyze the decomposition of the $(Bu^tO)_3SiOH$ precursor (c) through the formation of gaseous Bu^tOH by-products, allowing for the rapid deposition of ~12 nm of SiO_2 film per ALD cycle.

C. Aminosilanes

Unlike chlorosilane precursors, aminosilane precursors do not need a catalyst to enable SiO_2 ALD at <300 °C, reflecting their higher reactivity. Thermodynamically, amide ligands are predicted to be more reactive than chloro ligands for SiO_2 ALD by about 50–70 kJ/mol-ligand according to DFT cluster calculations.[6] Additionally, ALD of SiO_2 using aminosilane precursors is not expected to lead to particle formation (see discussion in Sec. II A), giving these precursors a distinct advantage versus chlorosilanes. The smallest homoleptic aminosilane, tetrakisaminosilane $Si(NMe_2)_4$, is found to be too sterically hindered for adsorption during ALD.[63] Other aminosilanes, $Si(NR_2)_x(H)_{4-x}$ $(1 \le x \le 3)$, can be classified as heteroleptic precursors, as they have a mix of amide and hydride ligands attached to the central Si atom. In these heteroleptic precursors, Si—H is such a strong, nonpolar bond that H rarely behaves as a hydride leaving group. Many studies have confirmed that loss of protonated amine is favored over loss of protonated hydride, i.e., H_2,[90–92] when these precursors adsorb onto —OH-terminated SiO_2 surfaces, as detailed below. It may, therefore, be appropriate to view the aminosilanes as a source of surface —SiH, $—SiH_2$, or $—SiH_3$. This $—SiH_x$ ($x = 1$, 2, or 3) terminated surface is quite inert toward reagents such as H_2O and requires temperatures >450 °C for complete oxidation by H_2O_2.[63] By employing more aggressive oxygen sources such as O_3 or O_2 plasma, deposition is enabled at <300 °C. High volume manufacturing PEALD processes for SAxP typically run at substrate temperatures <75 °C.[13,15] Ozone based processes are possible as low as 100 °C with sufficient flux of O_3.[91] The proposed reaction schematic for aminosilanes and O_3 or O_2 plasma is shown in Fig. 9. A modest thermal activation energy barrier has been computed to be necessary for the highly exothermic oxidation of H-terminated Si surfaces by O_3,[93,94] or O_2 plasma.[95] In both cases, the net effect was the insertion of O atoms into Si—H and regeneration of surface hydroxyl, which was experimentally confirmed by surface infrared spectroscopy.[63,91] Oxidation of ligands to hydroxyls at the surface is also observed in metal oxide ALD.[84]

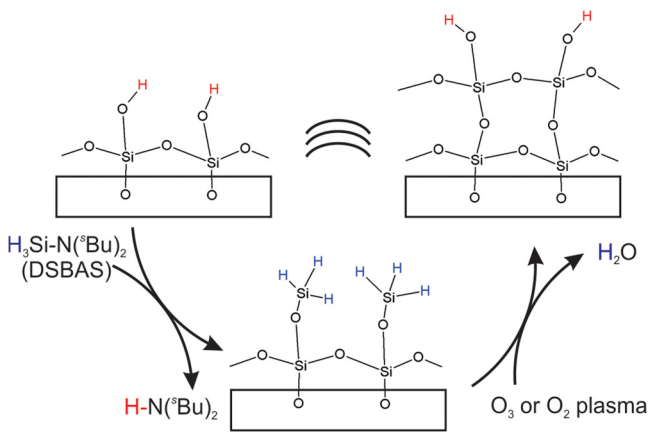

FIG. 9. Schematic ALD cycle at steady state for SiO_2 from pulses of the aminosilane precursor and the oxygen precursor (O_3 or O_2 plasma).

Understanding the routes to opening up Si—H bonds in this way may help in the search for ALD processes for SiC (see Sec. IV of this paper).

A key mechanistic question is how precursor performance is affected by the ratio of amide to hydride ligands. Tris(dimethylamino)silane ($SiH(NMe_2)_3$, TDMAS) would function as a source of SiH if it was to lose all three ligands as $HNMe_2$. However, it is computed by DFT that proton transfer and loss of the third amine ligand are kinetically and thermodynamically very unlikely under ALD conditions,[96] consistent with the infrared spectroscopic detection of this ligand at saturation by Kinoshita *et al.*[97,98] Oxidation of this remaining ligand in the O precursor pulse using, for example, O_3 may result in C and N impurities in the film. Bis(*tert*-butylamino)silane ($SiH_2(NH^tBu)_2$, BTBAS) is a potential source of SiH_2. Indeed, DFT calculations predict that the most favorable reaction pathway is for both amide ligands to be cleanly removed.[93] Elimination of both amide ligands was also computed with DFT for the $SiH_2(NR_2)_2$ precursors with R = Me (BDMAS)[95] and R = Et (BDEAS).[79,93] However, using transmission FTIR spectroscopy during SiO_2 ALD, Peña *et al.* showed that a fraction of the amine ligands remain on the SiO_2 surface following BTBAS chemisorption after the O_3 cycle, suggesting that not all of the amide ligands are removed during the surface reaction. This is due to the fact that a higher thermal activation barrier is computed for the second ligand elimination step than the first, which was verified later in a temperature-resolved experiment.[91] Han *et al.* showed that while the removal of the first ligand proceeds through the formation of a four-membered ring, the removal of the second ligand can occur through either the same pathway as the first or through the formation of a six-membered ring.[93] The formation of the six-membered ring was predicted to have a lower activation energy barrier but is less exothermic, suggesting that it would dominate at lower temperatures, while the formation of the four-membered ring would dominate at higher temperatures.[93] With just one amide ligand, di(*sec*-butylamino) silane ($SiH_3(N^{sec}Bu_2)$, DSBAS) should function as a source of SiH_3. DFT calculations show that ALD with O_3 is exothermic with low activation energy (25 kJ/mol).[94] Mallikarjunan *et al.* confirmed experimentally that DSBAS indeed shows ALD growth at lower temperatures than BTBAS or BDEAS.[99] They also found that DSBAS gives a higher GPC, which was explained by better surface packing of the SiH_3 fragment of DSBAS after elimination of a single amine, relative to the corresponding $SiH_2(NR_2)$ fragments of BTBAS or BDEAS.

The surface reaction mechanisms for the ALD of SiO_2 using aminosilanes and O_2 plasma or O_3 that were predicted by DFT calculations have been verified via surface infrared spectroscopy.[63,91,97] Figure 10 shows the infrared spectra of the DSBAS and O_2 plasma half-cycles during the ALD of SiO_2 at a substrate temperature of 400 °C obtained using ATR-FTIR spectroscopy. All half-cycle infrared spectra presented in this paper are difference spectra, meaning that a fresh background was collected prior to each precursor dose and that an increase or decrease in the infrared absorbance

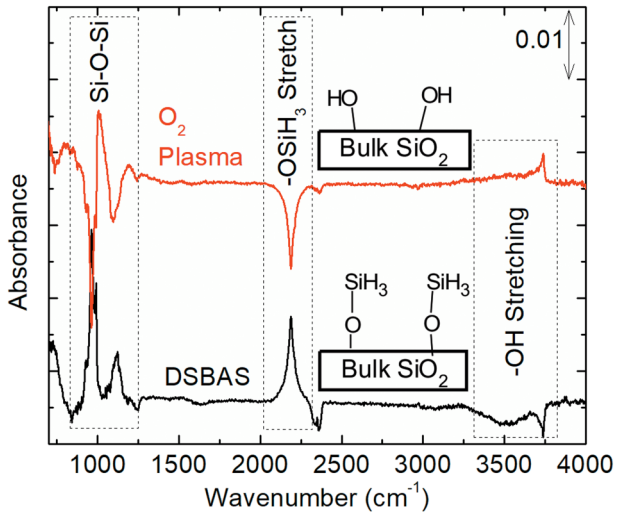

FIG. 10. Infrared absorbance change of DSBAS and O_2 plasma half-cycles during the ALD of SiO_2 at 400 °C. The surface termination following each precursor half-cycle is also shown.

corresponds to an increase or decrease in the number of species on the surface, respectively. On the post-O_2-plasma growth surface, DSBAS reacts with —SiOH surface species, as evidenced by the broad decrease at ~3600 cm^{-1} and the sharp decrease at ~3750 cm^{-1}, corresponding to the hydrogen-bonded and isolated —SiOH stretching vibrations, respectively.[63] The increase at ~2190 cm^{-1}, attributed to the —$OSiH_3$ stretching vibration,[100] suggests that the DSBAS reacts with the surface —SiOH species to form surface —$SiOSiH_3$ species, while the absence of a feature associated with the —CH_x ($x = 1$, 2, 3) stretching vibration at ~2900 cm^{-1} indicates that the amide ligand is the leaving group during the DSBAS chemisorption step, which is consistent with DFT calculations.[63,101] The increases associated with the Si—O—SiH_3 deformation vibrational modes[91] between 950 and 1100 cm^{-1} confirm that the DSBAS leaves behind a —$OSiH_3$ terminated surface. Therefore, the most likely gas-phase reaction product during the DSBAS half-cycle is di-sec-butylamine. In the O_2 plasma step, the —$OSiH_3$ surface species are removed, as evidenced by the decrease in the —SiH_3 stretching and deformation modes at ~2200 and 950–1100 cm^{-1}, respectively. SiO_2 film growth occurs during the O_2 plasma step as can be seen from the increase in the Si—O—Si phonon mode at ~1060 cm^{-1}.[63] The O_2 plasma also restores the surface —SiOH species, likely through either the insertion of O atoms into —SiH bonds, which is consistent with DFT, or through the recombination of surface H with O radicals generated in the plasma to form OH radicals that can react with the surface to provide surface —OH groups. A similar reaction mechanism was recently identified for the ALD of SiO_2 using DSBAS and O_3 by Peña *et al.*[91]

Murray *et al.* used DFT to quantify how the identity of the amide ligands in the aminosilane precursors affects the ALD mechanism.[6] The alkyl group (R) [for example, R = methyl (Me), ethyl (Et), isopropyl (^{i}Pr)] of the amide was observed to have a major effect during molecular adsorption of precursor via H-bonding with surface Si-OH on a —OH-terminated surface, presumably due to steric crowding at the surface. As a general rule, larger R groups were found to hinder adsorption, as seen in adsorption energies of −52, −42, −32 kJ/mol for R = Me, Et, ^{i}Pr in the $SiH_2(NR_2)_2$ precursor family. This could be ameliorated by replacing one R with H, e.g., −47 kJ/mol for R = ^{t}Bu in $SiH_2(NHR)_2$. All the DFT studies mentioned above find that molecular adsorption of aminosilanes is via H-bonding between surface hydroxyl and a precursor N atom. Han *et al.* calculated by DFT that the N—H interaction between the amine ligand in BTBAS and the surface hydroxyl has a bond length of 1.854 Å compared to 1.604 Å for TDMAS, implying weaker hydrogen bonding.[93] This was unexpected as TDMAS has three amide ligands while BTBAS has two, which would weaken the ability of the N atom to hydrogen bond due to the electron withdrawing alkyl groups. The longer bond length was explained by the steric repulsion from the bulky t-butyl groups, confirming that the identity of the amide ligand dictates precursor chemisorption. The studies also agree that the ALD reaction proceeds via concerted proton transfer from hydroxyl to amine and Si-O formation in four-membered ring structure at the TS (analogous to the structure shown in Fig. 5(a) for chlorosilane). The computed activation energy is of approximately the same magnitude as for chlorosilanes, with DFT studies of various aminosilanes in different surface models giving values over the range of 30–80 kJ/mol relative to the molecularly adsorbed state.[6,69,95,96] Therefore, in terms of reactivity for ALD of SiO_2, the amide ligands seem to behave similarly to chloro ligands, with quantitatively similar energetics for protonation. Both the processes based on chlorosilanes catalyzed by nucleophiles and those based on aminosilanes are viable at low temperatures, as evidenced by the chemisorption of BTBAS and DSBAS at 100 °C on —OH-terminated SiO_2.[91] As discussed above, in the chlorosilane case, this is understood as due to metastable intermediates where pentacoordinate Si is stabilized by a coadsorbed Lewis base ("cooperative effect," Fig. 7). We can, therefore, ask whether a similar mechanism is in operation for aminosilanes, especially since the HNR_2 by-product is Lewis basic and prone to remain H-bonded to the surface. On the other hand, amide ligands can be expected to be less electron-withdrawing than chloro ligands, disfavoring pentacoordinate Si. Unfortunately, none of the above DFT studies have clarified this by checking the effect of coadsorbed Lewis bases on the computed mechanism. It is also important to remember that surface amide ligands are prone to thermal decomposition. For example, β-hydride elimination of CH_4 from dimethylamide to yield an imide has been proposed based on surface infrared spectroscopy during ALD of SiO_2 from TDMAS and H_2O_2.[63] However, DFT studies have generally neglected to compute such pathways and analyze their effect on the overall surface reaction mechanism during ALD.

Based on the above discussion, it is clear that ALD of SiO_2 is at a mature stage of development. The reaction mechanisms that lead to film growth are relatively well understood, and processes that lead to high-quality, conformal SiO_2 deposition at low temperatures are already integrated

into the semiconductor device manufacturing. The next stage for the ALD of SiO_2 is, therefore, the improvement of existing processes to optimize parameters such as the GPC or the required precursor exposure, thereby increasing throughput or reducing the processing cost per wafer.

III. ATOMIC LAYER DEPOSITION OF SiN_x

In this section, we show that the ALD of SiN_x has been achieved using both thermal and plasma-assisted ALD processes. In contrast to the ALD of SiO_2, the low-temperature ALD of SiN_x remains problematic, with numerous challenges that must be overcome before these films can be fully integrated into semiconductor manufacturing. The primary challenge of thermal SiN_x ALD processes is the lack of N precursors reactive enough to enable SiN_x film growth at substrate temperatures <400 °C. To overcome these challenges, research into the ALD of SiN_x has changed focus from thermal to plasma-assisted SiN_x ALD processes. While SiN_x films have been deposited using both NH_3- and N_2-plasma-based ALD processes, there are still several issues associated with each approach. In NH_3-plasma-based ALD of SiN_x, the primary challenge is the relatively high H content of the deposited films, which leads to unacceptably high wet-etch rates, and nonisotropic etching in HAR nanostructures. In contrast, while N_2-plasma-based SiN_x processes deposit films that etch isotropically and have a low H content, the conformality of these films is typically <80% in HAR nanostructures.[102] Therefore, the integration of SiN_x films deposited using plasma-assisted ALD into semiconductor manufacturing will require fine-tuning of the current SiN_x deposition processes, whether by improving the stoichiometry of films deposited using H- and N-containing plasma ALD processes or by improving the conformality of N_2-plasma-based ALD processes. This could potentially be achieved via the use of more reactive Si precursors or through the introduction of multistep ALD processes.

For industrial applications, currently, ALD of SiN_x is achieved using a high-temperature thermal process from a chlorosilane precursor and NH_3.[103–106] However, low-temperature (≤400 °C) SiN_x ALD processes reported in the literature cannot provide the film attributes required for integration into semiconductor manufacturing.[47,49] Given the importance of developing new and improved SiN_x ALD processes, this section will provide a comprehensive overview of the SiN_x ALD processes currently reported in the literature (see Tables I and II). Recently, the literature on ALD of SiN_x was summarized in a review by Meng *et al.*[14] Therefore, in this review, we will primarily focus on the surface reaction mechanisms during SiN_x ALD with special emphasis on low-temperature (<400 °C), plasma-assisted ALD of SiN_x for single-wafer applications in semiconductor manufacturing.

Thermal and plasma-assisted ALD of SiN_x was first reported in the mid-1990s. The primary classes of Si precursor used for the ALD of SiN_x are chlorosilanes, aminosilanes, and silylamines, along with a few other silane derivatives. For thermal SiN_x ALD, only chlorosilanes such as SiH_2Cl_2, $SiCl_4$, and Si_2Cl_6 have been used as the Si precursors (see Table I). The N precursor is typically NH_3, or in a few studies N_2H_4 (see Table I). Plasma-assisted SiN_x ALD processes can be primarily classified into two categories: chlorosilanes with NH_3 plasmas and aminosilanes with N_2 plasmas (see Table II). SiN_x ALD with silylamine precursors has been reported with both NH_3 and N_2 plasmas. A plasma-assisted Si precursor step is obviously not possible as it would lead to continuous amorphous Si (*a*-Si) film growth.[143–145] For both the thermal and plasma-assisted approaches, the properties of the deposited films and the challenges associated with the ALD processes will be described in this section. In the case of thermal SiN_x ALD processes, the primary challenges are that high substrate temperatures and large precursor exposures are required: this is related to the low reactivity of the available N precursors. To overcome the challenges associated with thermal SiN_x ALD, semiconductor manufacturers are increasingly turning to plasma-assisted ALD processes.

TABLE I. Known thermal ALD processes for SiN_x.

Si precursor	N precursor	Temperature (°C)	GPC (Å)	Additional notes	Reference
$SiCl_4$	NH_3	427–627	2.4		107
$SiCl_4$	NH_3	375, 550–600	0.9–1.5	Temperature cycling	103, 104, 108–113
$SiCl_4$	NH_3	500	1.2		106
$SiCl_4$	NH_3	350–400	0.55		114
SiH_2Cl_2	NH_3	375, 550	0.9	Temperature cycling	115
SiH_2Cl_2	NH_3	500	1.2		106
SiH_2Cl_2	NH_3	450–550	0.8		105
Si_2Cl_6	NH_3	515–557	2.4–2.8		116
Si_2Cl_6	NH_3	300	0.55		117
Si_2Cl_6	N_2H_4	525–650	2.3		118
Si_2Cl_6	N_2H_4	285	–		119
Si_3Cl_8	NH_3	300–500	0.3–0.6		120

The transition to plasma-assisted ALD processes has introduced a unique set of processing challenges related to conformal deposition on high-aspect-ratio structures. Figure 11 shows the cross-sectional transmission electron microscopy (TEM) images of a typical SiN_x film grown by ALD on a nanostructure with an aspect ratio of ∼5. These SiN_x films were deposited at 375–400 °C. In Fig. 11(a), we see that the SiN_x film deposited using the chlorosilane and N- and H-containing plasma ALD process has a conformality >95%. This behavior is typical of ALD processes that use an N- and H-containing plasma.[11,47,49] After SiN_x deposition, the film shown in Fig. 11(a) was briefly immersed in a dilute HF solution (1% in H_2O) [Fig. 11(b)]. The etch rate in dilute HF can be used to probe the material differences between the planar and sidewall surfaces. The TEM micrograph in Fig. 11(b) shows that the planar surfaces of the SiN_x film remain intact, while the sidewall surfaces are completely etched away. In Fig. 11(c), the SiN_x film deposited using an aminosilane and N_2 plasma ALD process has a conformality of ∼50%. While values as high as ∼75% have been reported using bis(dimethylaminomethylsilyl)

TABLE II. Known plasma- and radical-assisted SiN_x ALD processes.

Si precursor	N plasma	Temperature (°C)	GPC (Å)	Additional notes	Reference
Chlorosilanes					
SiH_3Cl	NH_3	400	Not reported		10, 11
SiH_2Cl_2	NH_3	250–400	0.9		121, 122
SiH_2Cl_2	NH_3	375	1.0	Hot wire assisted	123
SiH_2Cl_2	NH_3	500	Not reported		10, 11
SiH_2Cl_2	NH_3	350–500	Not reported		124
SiH_2Cl_2	NH_3	350	0.24		125
SiH_2Cl_2	NH_3	400	~1		126
Si_2Cl_6	NH_3	350–450	1.2		47
Si_2Cl_6	NH_3 and N_2	300	0.5–1	Three-step process → Higher GPC	117
Si_2Cl_6	N_2/NH_3 and Ar/NH_3	270–360	0.6		127
$SiCl_2(CH_3)_2$	NH_3	475	Not reported		48
Aminosilanes					
BTBAS	N_2	80–500	0.16–0.93	GPC decreases with temp.	60, 128–130
3DMAS	N_2	350	0.11		125, 131
DSBAS	N_2	100–500	0.12–0.2	GPC decreases with temp.	62
DSBAS	N_2	225–375	0.5 ± 0.1		132
3DMAS	NH_3	350	No growth		125
BDEAS	NH_3	300	No growth		133
BDEAS	N2	225–375	0.5 ± 0.1		132
TEAS	NH_3	300	No growth		133
TIPAS	NH_3	300	No growth		133
DIPAS	NH_3	300	No growth		133
DIPAS	Ar and NH_3	300	0.4–0.7		133
DIPAS	N_2	60–250	0.4		134
DSN-2	N_2 and NH_3	250–500	0.43	Three-step process	135
Silylamines					
$N(SiH_3)_3$	N_2	250–300	1.2		61
$N(SiH_3)_3$	N_2	250	Not reported		125
$N(SiH_3)_3$	NH_3	150–350	0.68		136, 137
$N(SiH_3)_3$	N_2/H_2	300–400	1.3–2.1		28
DTDN2-H2	N_2	250–400	0.38		102, 138
Silanes					
SiH_4	N_2	250–400	0.06–2.5		139, 140
SiH_4	N_2/H_2	350	0.1		141
$Si(SiH_3)_4$	N_2	250–300	1.4		61
$SiH(CH_3)_3$	NH_3	300–450	0.7–0.8		142

trimethylsilyl amine with N_2 plasma,[102] almost all reports in the literature show that a lower film conformality is achieved in N_2-plasma-based processes compared to N- and H-containing plasmas. However, when SiN_x films grown using aminosilane and N_2 plasma processes are exposed to a dilute HF solution, the planar and sidewall surfaces remain primarily intact as shown in Fig. 11(d). The nonuniform SiN_x wet-etch rate for films deposited from cholorosilanes and the low conformality of the SiN_x film deposited from aminosilanes makes it difficult to integrate either process for applications in semiconductor manufacturing. Note that non-hydrogenated chlorosilane precursors, such as Si_2Cl_6, combined with N_2 plasma lead to poor quality SiN_x films that oxidize rapidly, and hydrogenated chlorosilanes combined with N_2 plasmas again lead to poor conformality. On the other hand, processes that use aminosilanes combined with NH_3 plasma simply do not deposit SiN_x films under self-limiting conditions.[133] To explain the challenges associated with thermal and plasma-assisted SiN_x ALD processes, a better understanding of the surface reaction mechanisms for the ALD of SiN_x is required.

In the rest of this section, we focus on identifying the surface reaction mechanisms for three primary classes of Si precursor used in SiN_x ALD: chlorosilanes, silylamines, and aminosilanes. We then use these surface reaction mechanisms to explain the differences in film properties between SiN_x films deposited using these classes of ALD precursors.

A. Chlorosilanes

Chlorosilanes were the first class of Si precursor that were extensively used for SiN_x ALD, first with NH_3 in thermal

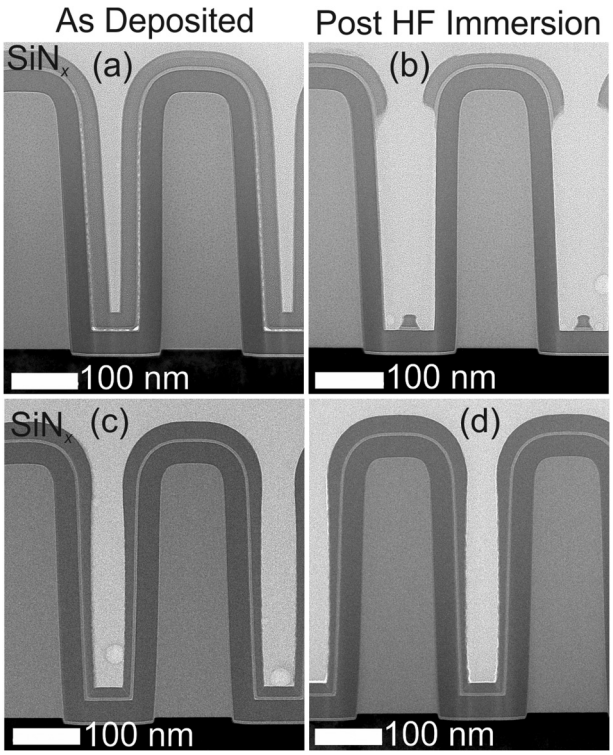

FIG. 11. Cross-sectional TEM images of an SiN_x film deposited using a chlorosilane and NH_3 plasma ALD process before (a) and after (b) immersion in a dilute aqueous HF solution for 30 s, and an SiN_x film deposited using an aminosilane and N_2 plasma ALD process before (c) and after (d) immersion in a dilute aqueous HF solution for 30 s.

processes and later with NH_3 plasmas to lower the growth temperature. Table I shows the chlorosilane precursors, growth temperatures, and GPC values for various thermal SiN_x ALD processes reported in the peer-reviewed literature prior to January 1, 2019 obtained via Web of Knowledge™. As can be seen from Table I, thermal ALD of SiN_x chlorosilanes is based on NH_3, or rarely, N_2H_4 as the N precursors. Chlorosilanes are preferred in thermal processes over aminosilanes since $-SiH_{(3-x)}(NRR')_x$ ($x = 0$–3) terminated surfaces created by aminosilanes are not very reactive with either NH_3 or N_2H_4 (or with H_2O or H_2O_2, as already noted in Sec. II C).[128,129,146]

Figure 12 shows a typical reaction schematic for SiN_x film growth using $SiCl_4$ with either thermal NH_3 or NH_3 plasma. During the Si precursor pulse $SiCl_4$ interacts with $-NH_x$ ($x = 1$, 2) surface species created by the reaction of NH_3 or due to exposure to an NH_3 plasma. The reaction of $SiCl_4$ with this surface is proposed to proceed though the formation of an overcoordinated Si center, as already discussed for the chlorosilane SiO_2 processes (see Sec. II A).[6,117] In the reaction, surface $-SiCl_x$ ($x = 1$, 2, 3) species are created as one or more of the Cl ligands are removed through the formation of HCl as the volatile reaction by-product which may remain on the surface or desorb into the gas phase and be pumped away. In the subsequent thermal NH_3 half-cycle, the N precursor reacts with the $-SiCl_x$ ($x = 1$, 2, 3) surface, to form an $-NH_x$ ($x = 1$, 2) terminated surface with HCl again released as the volatile reaction by-product. A similar

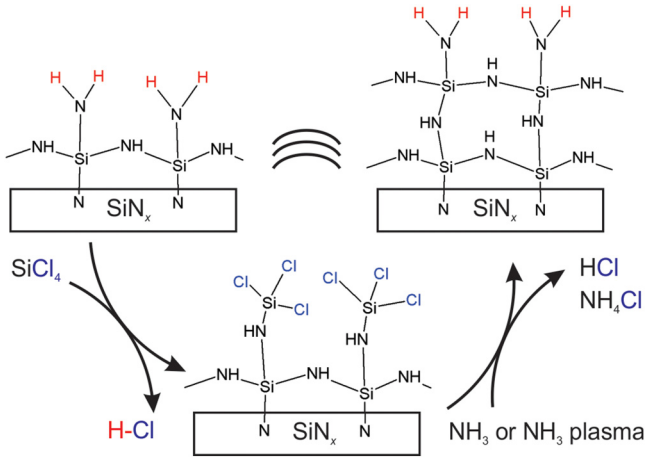

FIG. 12. Schematic ALD cycle at steady state for SiN_x from pulses of cholorosilane precursor and N precursors (NH_3 or NH_3 plasma).

surface termination is observed in experiments for NH_3 plasmas, but the reaction mechanism is expected to be very different due to the presence of radicals in the plasma step, which likely undergo redox reactions rather than acid-base reactions. The formation of HCl during the N precursor step presents a unique problem. First, HCl is a corrosive gas, which complicates material requirements for the reactor. Second, unreacted NH_3 and the HCl by-product react to form NH_4Cl.[47] While NH_4Cl is not stable at the growth temperature of SiN_x, which is usually >300 °C for chlorosilane precursors (see Table I), this salt has the potential to accumulate on any cold surfaces in the reactor and can eventually lead to particulate formation.

The surface reaction pathways shown in Fig. 12 that leads to SiN_x film growth during thermal ALD from $SiCl_4$ and NH_3 were validated by Klaus *et al.* using transmission FTIR spectroscopy (see Fig. 13).[107] Klaus showed that on the $-NH_2$-terminated surface obtained after the NH_3 cycle, $SiCl_4$ reacts with surface $-NH_2$ species, as can be seen from the decrease in absorbance for the $-NH_2$ scissor mode at ~1550 cm^{-1} in Fig. 13. The corresponding increase in absorbance for the $-SiCl_2$ stretching vibrations at ~600 cm^{-1} in Fig. 13 shows that the surface reaction of $-NH_2$ with $SiCl_4$ produces a $-SiCl_2$-terminated surface, with HCl released as the reaction by-product. In the subsequent step, the $-SiCl_2$ surface species react with NH_3 to restore the $-NH_2$-terminated surface. While Klaus *et al.* did not show that $SiCl_4$ reacts with surface $-NH$ species, the low H content reported for their SiN_x films suggests that $SiCl_4$ also reacted with surface $-NH$ groups.[107] However, this ALD process used very large precursor doses, ~10^{10} L. It is clear from previous experiments that more reactive N precursors or substantially extended N precursor doses are required. More reactive N precursors such as N_2H_4 are difficult to handle due to safety concerns, which necessitates the use of NH_3 requiring doses as high as 10^8–10^{10} l.[14,47]

Plasma-assisted processes can overcome the requirement of high temperatures and large NH_3 doses associated with thermal SiN_x ALD processes: this is made possible by

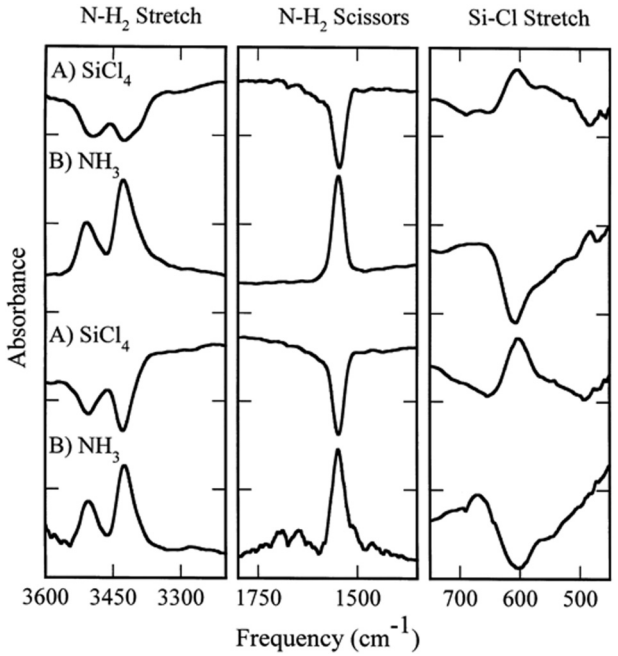

FIG. 13. Half-cycle infrared absorbance change spectra for an SiN_x ALD process using $SiCl_4$ and NH_3 at 427 °C. Reproduced with permission from Klaus *et al.*, Surf. Sci. **418**, L14 (1998) (Ref. 107). Copyright 1998 Elsevier.

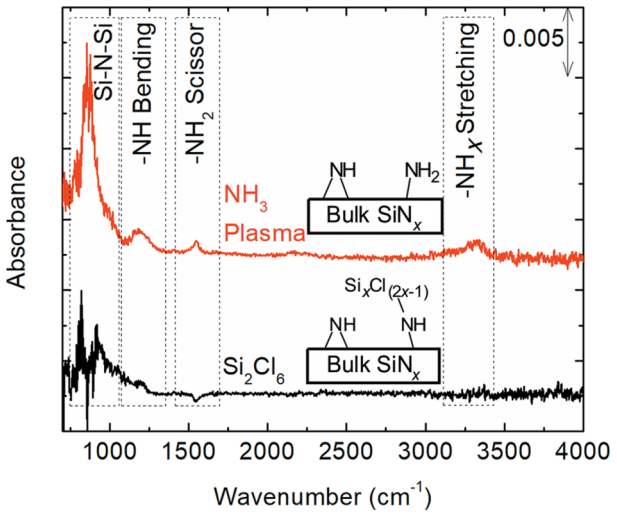

FIG. 14. Infrared absorbance change for the Si_2Cl_6 and NH_3 plasma half-cycles during ALD of SiN_x at 400 °C. The surface termination following each precursor half-cycle is also shown.

enhancing the reactivity of the N precursor step using radicals generated in NH_3, N_2, or N_2/H_2 plasmas.[13] Table II summarizes the peer-reviewed literature on plasma-assisted ALD of SiN_x up to January 1, 2019, obtained via Web of Knowledge™. The addition of the plasma step means that the chlorosilane half-cycle dictates the lowest temperature at which the ALD of SiN_x can be achieved. The lowest temperature reported for chlorosilane/NH_3 plasma ALD process is 300 °C. While chlorosilane and NH_3 plasma-based ALD processes enable low-temperature growth, the SiN_x films tend to have a high H content, typically on the order of 20 at. %.[47,49] This leads to suboptimal film properties such as low mass density and a high wet-etch rate in dilute HF. The primary method of H incorporation into SiN_x films deposited using most precursors and plasmas has been reported as —NH species, while —SiH_x ($x = 1, 2, 3$) species are generally absent.[47] To understand how H is incorporated in bulk SiN_x during ALD, it is first important to identify the half-reactions during growth.

Recently, using surface infrared spectroscopy, Agarwal and co-workers studied the half-reactions during Si_2Cl_6 and NH_3 plasma ALD process for SiN_x. Figure 14 shows the infrared absorbance change for the Si_2Cl_6 and NH_3 plasma half-cycles during the ALD of SiN_x at 400 °C obtained using *in situ* ATR-FTIR spectroscopy.[47] Following an NH_3 plasma half-cycle, the infrared spectrum for the Si_2Cl_6 half-cycle shows that on the SiN_x growth surface, Si_2Cl_6 reacts primarily with —NH_2 surface species as evidenced by the decrease in the —NH_2 scissor mode at 1550 cm^{-1}.[147] A corresponding increase in the —NH bending mode at ~1180 cm^{-1} suggests that Si_2Cl_6 reacts with —NH_2 surface species to form —NH and —Si_xCl_{2x-1} ($x = 1, 2$) surface groups.[148] Because the spectral cutoff of the ATR-FTIR setup is ~700 cm^{-1}, and the —$SiCl_x$ ($x = 1, 2, 3$) stretching modes appear at ~600 cm^{-1},[149] these vibrational modes were not directly observed in these infrared spectra. However, as discussed above, from transmission FTIR spectroscopy, Klaus *et al.* showed that —$SiCl_x$ ($x = 1, 2, 3$) stretching vibrations are observable after $SiCl_4$ chemisorbs onto a —NH_x ($x = 1, 2$) terminated surface: this suggests that surface —Si_xCl_{2x-1} ($x = 1, 2$) should be present after the chemisorption of Si_2Cl_6.[107] In the subsequent NH_3 plasma half-cycle, Cl and possibly some Si from the —Si_xCl_{2x-1} ($x = 1, 2$) surface groups would be removed by the reactive species generated in the NH_3 plasma. The NH_3 plasma half-cycle also restores the surface —NH_2 species as is seen due to the increase in the —NH_2 scissor mode at 1550 cm^{-1},[147] which allows for the continuation of the ALD process. It should be noted that even though the NH_3 plasma contains atomic H radicals,[150] few —SiH_x ($x = 1, 2, 3$) species are formed during the plasma step. The NH_3 plasma also incorporates a substantial amount of —NH species, as evidenced by the increase in the —NH bending mode at 1180 cm^{-1} and the —NH_x ($x = 1, 2$) stretching mode at ~3300 cm^{-1}. In this ALD process, the surface —NH species created during the NH_3 plasma half-cycles remain unreacted during the Si_2Cl_6, half-cycles. In addition, surface —NH_2 groups react readily with Si_2Cl_6 to convert to unreactive —NH groups,[151] which explains the generally high H content, ~20%, of the SiN_x films deposited using this class of ALD processes.

B. Silylamine and aminosilanes

To lower the H content of plasma-assisted SiN_x ALD processes and therefore improve the film quality, more reactive Si precursors have been tested. The first of these, TSA [$N(SiH_3)_3$], is a highly reactive Si precursor that has been used for both NH_3- and N_2-plasma-based SiN_x ALD processes. The reaction pathway proposed for TSA in an SiN_x

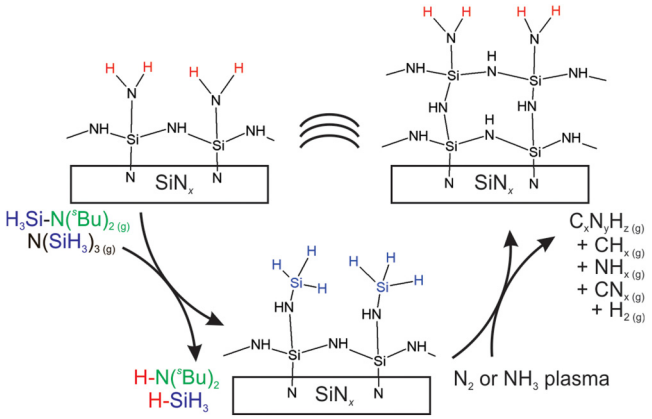

FIG. 15. Schematic ALD cycle at steady state for SiN_x from pulses of aminosilanes or trisilylamines, and NH_3 or N_2 plasmas.

plasma ALD process is shown in Fig. 15. In this pathway, TSA reacts with $-NH_x$ ($x = 1, 2$) surface species to form an $>NSiH_3$-terminated surface with SiH_4 liberated as the gas-phase reaction by-product. This makes the surface termination following TSA chemisorption similar to what is expected for aminosilane precursors such as DSBAS and is the reason why we chose to place this precursor in the same category as aminosilanes in Fig. 15. In the subsequent NH_3 plasma half-cycle, the $>NSiH_3$ surface species are removed and the $-NH_x$ ($x = 1, 2$) surface is restored. Using ATR-FTIR spectroscopy, we experimentally validated the surface reaction pathway proposed in Fig. 15 for the TSA and NH_3 plasma ALD process, as outlined next.

Figure 16 shows the infrared difference spectra of the TSA and NH_3 plasma half-cycles at 400 °C obtained using ATR-FTIR spectroscopy. In the spectrum for the TSA half-cycle, the increase at $\sim 2180\,cm^{-1}$ can be assigned to the $>NSiH_3$ stretching mode.[100] From the corresponding decrease in absorbance for the $-NH$ bending mode at

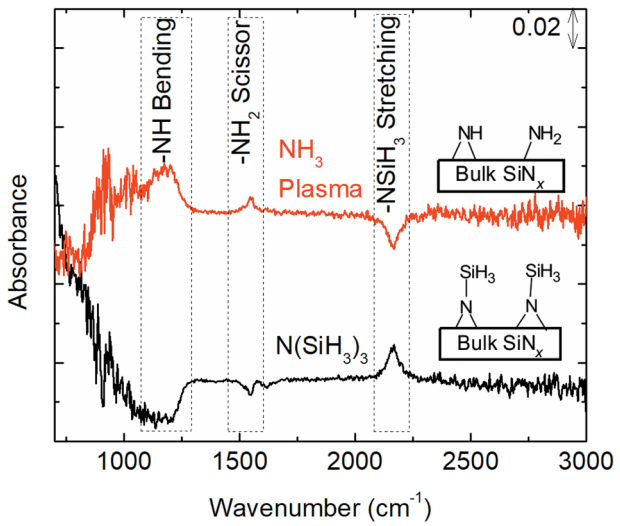

FIG. 16. Infrared absorbance change during the TSA and NH_3 plasma half-cycles of the SiN_x ALD process at 400 °C. The surface termination following each precursor half-cycle is also shown.

$\sim 1180\,cm^{-1}$ and the $-NH_2$ scissor mode at $\sim 1550\,cm^{-1}$, it is evident from the TSA reacts with both $-NH$ and $-NH_2$ surface species on the post-NH_3-plasma treated SiN_x growth surface[147,148] to form $>NSiH_3$. This is unlike the previously described Si_2Cl_6 and NH_3 plasma SiN_x ALD process where the Si precursor reacts preferentially with surface $-NH_2$ groups. In the subsequent NH_3 plasma half-cycle, the infrared spectrum clearly shows that surface $>NSiH_3$ is removed, and $-NH$ and $-NH_2$ surface species are restored, allowing for the continuation of the ALD process. As TSA reacts with both $-NH$ and $-NH_2$ surface species, the SiN_x films deposited using this precursor tend to have a hydrogen content that is approximately half of that obtained using chlorosilane and N- and H-containing plasmas.[28,136,137] Additionally, SiN_x films grown using TSA and NH_3 plasma exhibit excellent conformality. While there are reports of SiN_x films deposited using TSA and N_2 plasma, the conformality of these films has not been reported, but is expected to show similar trends to that of other N_2-plasma-based processes (see Fig. 11). Despite its higher reactivity, the application of TSA as a potential precursor suffers from several disadvantages. First, TSA is substantially more expensive than chlorosilanes and aminosilanes.[152] Second, the required dose for TSA is substantially larger than that for chlorosilanes, which makes using TSA even more expensive.[152] Third, TSA is highly pyrophoric, which introduces additional safety concerns. Therefore, researchers have turned to other classes of Si precursors.

Due to their higher reactivity, aminosilanes are an alternative to chlorosilanes and silylamines.[117,153] Additionally, unlike chlorosilanes, aminosilanes do not form highly corrosive reaction by-products such as HCl. For plasma-assisted SiN_x ALD, it turns out that aminosilane precursors can only be used in conjunction with N_2 plasmas. Aminosilane precursors with NH_3 plasmas do not lead to film growth for reasons that are not completely understood.[133] We will address this observation later in this section. Similar to TSA, aminosilane chemisorption produces surface silicon hydrides as it creates a $-SiH_{(3-x)}(NR_2)_x$ ($x = 0$–3) terminated surface, but distinct in the sense that unreacted amide ligands can be present on the surface as well, depending on the number of amide ligands in the aminosilane precursor. The most commonly used aminosilane precursors contain one or two amide ligands.[14] This surface is then exposed to an N_2 plasma in the following half-cycle. While no H-containing radicals are expected in an N_2 plasma, this step still creates surface $-NH_x$ ($x = 1, 2$) species due to the recycling and redeposition of H atoms present on the surface following the aminosilane chemisorption step.[60] Recently, Agarwal co-workers showed that during SiN_x ALD from aminosilanes and N_2 plasma, surface aminosilanes react with surface $-NH$ groups created after the N_2 plasma half-cycle. This is similar to the reaction of TSA with surface $-NH$ groups (see Fig. 16) after the NH_3 plasma half-cycle.[132]

Figure 17 shows the infrared spectrum of an SiN_x film deposited using BDEAS and N_2 plasma at 375 °C. The prominent feature at $\sim 870\,cm^{-1}$ corresponds to the Si—N—Si phonon mode.[148] The two features at ~ 1180 and

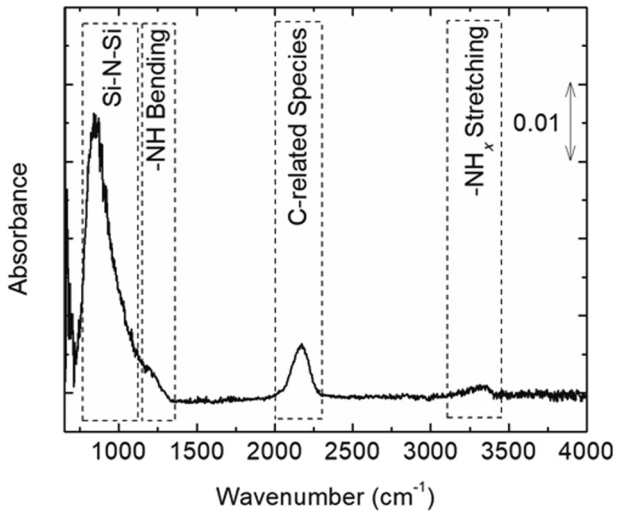

FIG. 17. Infrared spectra of an SiN_x film deposited using BDEAS and N_2 plasma at 375 °C. The feature at ~2180 cm^{-1} represents redeposited C-containing species.

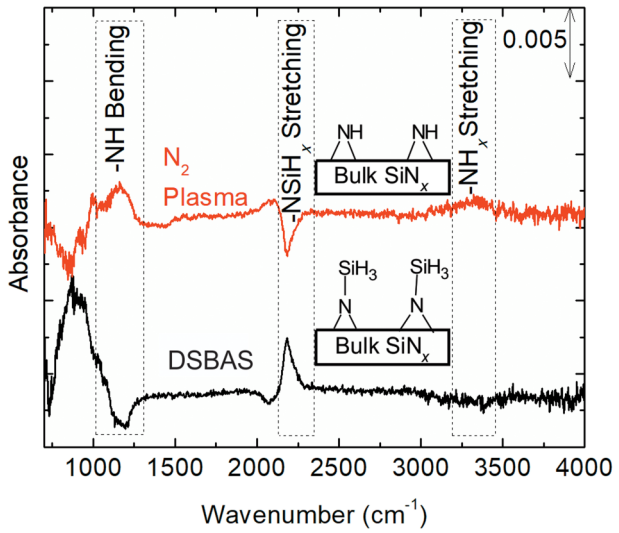

FIG. 18. Infrared absorbance change during the DSBAS and N_2 plasma half-cycles during ALD of SiN_x at 375 °C. The surface termination following each precursor half-cycle is also shown.

~3300 cm^{-1} are attributed to the —NH bending mode and the —NH_x ($x = 1$, 2) stretching mode, respectively. These vibrational features in Fig. 17 are typical of SiN_x films deposited using low-temperature ALD processes,[47,49,128–130] with the exception of the feature at ~2180 cm^{-1}. In SiN_x films, this feature is generally assigned to the —SiH_x ($x = 1$, 2, 3) stretching vibrations. However, we assigned this band to C-related species, as described previously.[49] Similar to surface —NH_x ($x = 1$, 2) species, the presence of C-related species after the N_2 plasma half-cycle is also attributed to abstraction and redeposition of surface atoms by radicals and ions generated in the plasma following the BDEAS precursor half-cycle.[60] Using optical emission spectroscopy, Knoops *et al.* showed that in a BTBAS and N_2 plasma ALD process, the CN* emission line at ~388 nm undergoes time-dependent decay during the plasma step. A plausible explanation for the transient CN* emission is that in the initial stages of the plasma half-cycle, carbon-containing surface species are abstracted by the N radicals in the N_2 plasma. These C- and N-containing species desorb from the surface and likely undergo electron-impact reactions in the plasma to produce CN radicals that impinge onto the surface.[60] As the surface reservoir of carbon depletes during the N_2 plasma half-cycle, CN* emission also decays. This recycling of carbon from the surface into the plasma and then back to the surface is governed by the gas residence time and becomes less prominent at lower residence times. The redeposition effect is expected to play a lesser role in NH_3-plasma-based processes due to the presence of a substantial amount of atomic H that can potentially remove redeposited species.[150] Next, we look at the reaction mechanism for DSBAS and N_2 plasma.

Figure 18 shows the infrared spectra for the DSBAS and N_2 plasma half-cycle for SiN_x ALD at 375 °C. On the SiN_x growth surface following an N_2 plasma step, DSBAS reacts primarily with —NH surface species as evidenced by the decrease in the —NH bending mode at ~1180 cm^{-1}.[148,154] The —NH species are created on the surface due to the redeposition effect described previously. Unlike the Si_2Cl_6 and NH_3 plasma ALD process (see Fig. 15), a substantial amount of —NH_2 surface species is not present on the surface following the N_2 plasma half-cycle. Therefore, there is no observable decrease in the —NH_2 bending mode, even though —NH_2 surface species are more reactive than —NH surface species. The increase at ~2170 cm^{-1} is indicative of the —$NSiH_3$ stretching vibration and corresponds to —SiH_3 surface species formed by DSBAS chemisorption.[100] The absence of a —CH_x ($x = 1$, 2, 3) stretching vibration at ~2900 cm^{-1} shows that the single amine ligand from DSBAS is the leaving group during chemisorption.[101,155] In the subsequent N_2 plasma half-cycle the —SiH_3 surface species are removed, and the —NH surface species are restored, as seen by the increase in the —NH bending and stretching mode at ~1180 and ~3300 cm^{-1}, respectively, allowing for the continuation of the ALD cycles. Unlike the Si_2Cl_6 and NH_3 plasma ALD process where Si_2Cl_6 preferentially reacts with only surface —NH_2 groups, the more reactive DSBAS precursor reacts readily with —NH surface species. Efficient reaction of the aminosilane with surface —NH groups, combined with the fact that the N_2 plasma does not bring much H to the SiN_x surface, very little H is incorporated into the SiN_x films (<5%). This low level of H incorporation could be used to explain why SiN_x films deposited using aminosilane precursors and N_2 plasmas exhibit good material properties and respond uniformly to wet etching in a dilute HF solution (see Fig. 11).[62] It should be noted that this reaction mechanism contradicts the one proposed recently by Peña *et al.*, where they suggested that the primary reactive sites for the chemisorption of DSBAS are undersaturated Si atoms, i.e., dangling bonds.[156] While dangling bonds are expected to be highly reactive surface sites,[157] we contend that their presence on the surface after the N_2 plasma step is highly unlikely as background H_2O and O_2 would immediately react with these dangling bonds sites after the N_2 plasma is turned off.

Using gas-phase transmission FTIR spectroscopy, Bosch *et al.* verified that primary amines are the gaseous reaction by-product during the chemisorption of the aminosilane precursor.[128] The infrared spectra from Bosch *et al.* reproduced in Fig. 19 clearly show that following BTBAS chemisorption after the N_2 plasma half-cycle, *tert*-butylamine [$NH_2C(CH_3)_3$] is the reaction by-product. This is consistent with the reaction of DSBAS with surface —NH groups that were inferred from the surface infrared spectra shown in Fig. 18, and this surface reaction will lead to the formation of amines as the reaction by-product.

A comparison of the reaction mechanisms for the three selected ALD processes provides some explanation of the experimentally observed SiN_x film properties. The first observation is that the H content of the deposited SiN_x films is governed by both the reactivity of the Si precursor and whether the N-containing plasma contains H. In the case of the Si_2Cl_6 and NH_3 plasma ALD process, the Si_2Cl_6 is not reactive enough to react with —NH surface species at low temperatures, and the NH_3 plasma contains a substantial amount of H, leading to typical atomic H contents of ~20%.[47,49] In the TSA and NH_3 plasma ALD process, while the NH_3 plasma still contains H, the TSA precursor is reactive enough to remove both —NH and —NH_2 surface species leading to a lower H content of ~13%.[136,137] Finally, in the DSBAS and N_2 plasma half-cycle, DSBAS reacts with —NH surface species, while —NH_2 surface species do not appear to be present. Due to the lack of atomic H in N_2 plasmas, and the reactivity of aminosilanes with surface —NH, the typical atomic H content in SiN_x films is ~5%.[62,129] The H content of the SiN_x films then determines several other properties, such as the refractive index, the film density, which both tend to decrease with increasing H content. The observed trends in the H content of the deposited films could potentially explain the nonisotropic etching seen in Fig. 11.

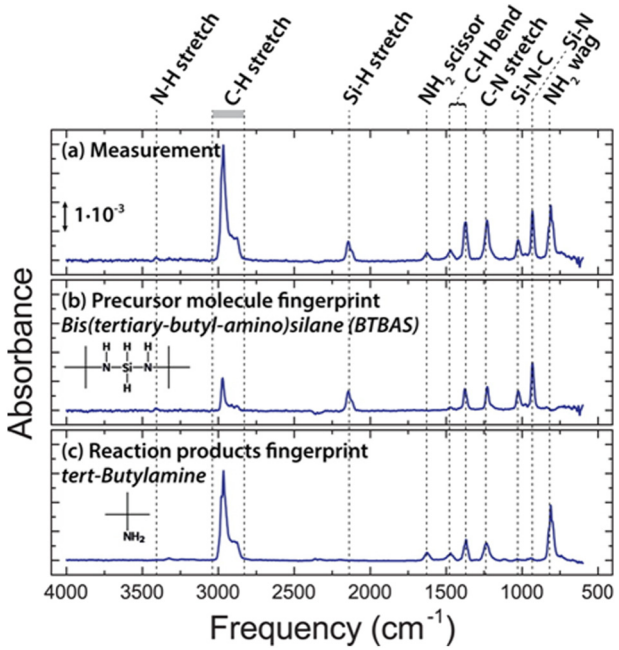

FIG. 19. (a) Gas-phase IR spectrum during the BTBAS half-cycle for N_2-plasma-assisted ALD of SiN_x. (b) Gas-phase infrared spectrum of the BTBAS molecule. (c) Vibrational fingerprint of the primary reaction product during the BTBAS half-cycle identified as *tert*-butylamine. All three graphs are plotted on the same scale. Reprinted with permission from Bosch *et al.*, Chem. Mater. **28**, 5864 (2016) (Ref. 128). Copyright 2016 American Chemical Society.

In plasma-assisted SiN_x ALD processes, the differences in conformality of the as-deposited SiN_x films have been attributed to several factors. A possible explanation is that the radicals produced in the NH_3 plasma such as NH and NH_2 are more likely to diffuse to the bottom of the trench, compared to the N radicals produced in an N_2 plasma, leading to greater conformality. As radicals diffuse down the trench in a nanoscale feature, they collide with the sidewalls, meaning that a species that is less likely to react with or recombine on the wall will make it further down the trench. This may explain the observations of Faraz *et al.* who showed that increasing the N_2 plasma duration in a DSBAS and N_2 plasma SiN_x ALD process did not necessarily lead to an improvement in SiN_x film conformality.[62] The response of the SiN_x films to the dilute HF solution can be attributed to directional ion bombardment. Ion-bombardment affects primarily the planar surfaces densifying them due to the physical removal of H-containing species. The direction ion-bombardment effect is very clear from the small feature remaining on the planar surface at the bottom of the trench in Fig. 11(b). However, since both the NH_3 and N_2 plasma contain ions of a similar mass, the SiN_x films in Fig. 11(a) should respond to the dilute HF in a way that is similar to the film shown in Fig. 11(c). Since this is not the case, we argue that the wet-etch response of the SiN_x films with increasing H content is most likely very nonlinear. It is likely that the H content of the sidewalls in chlorosilane and NH_3 plasma ALD processes is even higher than ~20% due to lower ion bombardment, as most ions arrive at near-normal incidence toward the substrate. Even though the planar surfaces with a high H content of up to 20% can sustain wet etching in dilute HF, we speculate that the sidewall surfaces have an H content that is not only higher, but also above a certain critical threshold, which leads to complete etching of the sidewall surfaces in HF. While the sidewall H content of films deposited by N_2 plasma-assisted ALD may be slightly higher than the ~5% atomic H measured on planar surfaces, the value is most likely well below the threshold where H content strongly influences the wet-etch rate.[47,49,62,129]

IV. ATOMIC LAYER DEPOSITION OF SiC

The ALD of SiC has proven to be extremely challenging, more so than SiO_2 and Si_3N_4.[158] The few existing thermal processes reported as ALD in the literature are usually operated at substrate temperatures >800 °C. These high-temperature processes report GPCs much greater than 2 Å, which suggests that they may not be self-limiting and that a CVD component is likely playing an important role during film growth. Although these processing conditions would complicate the integration of these processes into the modern semiconductor manufacturing flow, it is important to note

that unlike the *a*-SiC films relevant to the semiconductor industry today, the focus of these early studies summarized in Table III was on the atomic layer epitaxy of single crystalline SiC films. Plasmas cannot be used to lower the growth temperature, because unlike SiO_2 and SiN_x ALD, the reaction of plasmas containing precursors for either Si or C do not self-limit and both lead to continuous film growth. This in turn necessitates that both the Si and C precursor half-cycles are driven thermally.

Table III shows the precursors, growth temperatures, and GPCs of the thermal SiC ALD processes reported in the peer-reviewed literature prior to January 1, 2017 obtained via Web of Knowledge™. The most common Si precursor is Si_2H_6 with C_2H_2 or C_2H_4 as the C source: the exceptions are Nagasawa *et al.* who used SiH_2Cl_2 and C_2H_2,[164,165] and Sadayuki *et al.*[166] who used $SiH_2(C_2H_5)_2$ as a single-source precursor. As can be seen in Table III, almost all of the SiC ALD processes with the exception of that of Sadayuki *et al.* have GPCs greater than 2 Å, which is uncharacteristically high for ALD processes. It should also be noted that the reported temperatures for these ALD processes is greater than the thermal decomposition temperature of the surface species created after the reaction of Si_2H_6, C_2H_2, and C_2H_4 precursors.[101,167] In particular, H desorption from Si surfaces starts to occur at >350 °C,[168] and it has also been reported that at above 423 °C, methyl groups adsorbed on an Si surface begin to decompose through an H elimination mechanism.[101] This may indicate that growth is occurring via pulsed CVD, where the GPC is controlled by precursor exposure rather than self-limiting surface reactions. In the case of Nagasawa *et al.*, the use of a chlorosilane precursor, which is generally more reactive than unsubstituted silanes, did not result in a substantial lowering of the deposition temperature. Sadayuki *et al.* pursued an alternative approach using a single-source precursor, $SiCl_2(CH_3)_2$, that contains both Si and C atoms. However, it is not clear how a single-source process can be self-limiting, especially at the reported growth temperature. The high temperatures required to grow SiC films in these cases indicate that the reaction of $-SiH_xCl_{(3-x)}$ ($x = 0$–3) surface species with the gaseous C_2H_2 or C_2H_4 precursors or the reaction of $-CH_x$ ($x = 1$, 2, 3) surface species with gaseous Si_2H_6 is kinetically or thermodynamically unfavorable. This has been partially confirmed by Gutleben *et al.* who showed that CH_3I, a precursor expected to be more reactive than other halomethane precursors,[169,170] does not react significantly with an H-terminated Si(100)–2 × 1 surface.[171] Since iodomethanes do not seem to react with $-SiH_x$ ($x = 1$, 2, 3) terminated surfaces, it is unsurprising that the currently tested SiC precursors have been unsuccessful for ALD and that more reactive precursors are needed to create surface terminations that can enable the ALD of SiC at lower temperatures. Additionally, the presence of a methyl group on Si has been shown to effectively passivate the Si, which means that $-CH_x$ ($x = 1$, 2, 3) surface functionalization makes the surface unreactive to subsequent Si precursor steps.[172]

TABLE III. Precursors and film properties of the known thermal SiC ALD processes.

Si precursor	C precursor	Temperature (°C)	GPC (Å)	Reference
Si_2H_6	C_2H_2	1000–1050	4–7	159, 160
Si_2H_6	C_2H_2	1050	4–5	161, 162
Si_2H_6	C_2H_4	850–980	2.1	163
SiH_2Cl_2	C_2H_2	800–1050	4–9	164, 165
$(C_2H_5)_2SiH_2$	—	590–675	0.2	166

In a recent article, Filatova *et al.* used *ab initio* DFT to calculate the Gibbs free energy (ΔG) of reactions for a broad spectrum of Si and C precursors for the low-temperature thermal (400 °C) ALD of SiC.[66] Their calculations suggested that in terms of thermodynamics, the most promising precursors for the ALD of SiC at 400 °C were SiH_4, Si_2H_6, or SiH_3Cl combined with C_2H_2, CCl_4, or $CHCl_3$ as the Si and C precursors, respectively.[66] However, several of the precursors with the most negative ΔG have been tested experimentally and do not lead to low-temperature ALD of SiC. This suggests that activation energy barriers for the reaction (which were not computed in the study) are too high. Therefore, to enable SiC ALD, it is likely that entirely new classes of Si and C precursors have to be designed and tested in the future.

The difficulty of depositing an SiC film using thermal ALD processes has forced researchers to pursue alternative solutions, such as the incorporation of C into Si-based dielectric films such as SiO_2 and SiN_x to form ternary blends of SiCO and SiCN, respectively. However, this alternative also remains challenging with very few reports on the ALD of SiCO and SiCN.[173–175] Below, we summarize some of the challenges associated with the incorporation of C into Si-based dielectric films.

Kim *et al.* reported plasma-assisted ALD of low-*k* SiCO using dimethoxydimethylsilane (DMDMS: $C_4H_{12}O_2Si$) and $C_6H_{10}O$ as the precursors.[175] The 8–16 Å GPC for this process indicates that this is a pulsed CVD rather than self-limiting ALD. This is corroborated by the fact that DMDMS has been used as a single-source precursor for the plasma-enhanced CVD (PECVD) of SiCO.[176] In a similar study, Lee *et al.* used sequential exposures of a trimethylsilane (TMS: $SiH(CH_3)_3$) plasma and O_2 plasma for the ALD of SiCO.[174] Lee showed using FTIR spectroscopy that as the rf power to the TMS plasma was increased from 100 to 500 W, the amount of C incorporated into the film increased. However, similar to the process used by Kim *et al.* described above, the GPC was ~8 Å, which suggests that this process is not true ALD but rather PECVD. Again, TMS is a known PECVD precursor for Si- and C-containing films.[177]

In order to achieve ALD of SiC_xN_y, Kim *et al.* used an aminosilane precursor, bis(dimethylamino)dimethylsilane, combined with an H_2 plasma to deposit SiC_xN_y films at substrate temperatures of 150 and 300 °C.[173] Kim *et al.* showed that the deposited SiC_xN_y film had a low conformality. The Si/C ratio was reported as ~1 at 300 °C. From the article, it is difficult to assess the quality of the SiC_xN_y film or to identify whether the preferred C bonding configuration of

Si—C—Si, which provides oxidation resistance, is present within the SiC_xN_y matrix.[173]

Figure 20 shows a few hypothetical pathways for incorporation of C into SiN_x and SiO_2 films through modification of known ALD processes for SiN_x and SiO_2.[48] In the first approach, it is hypothesized that C can be incorporated into an SiN_x film through the use of an Si precursor with Si—C bonds followed by an NH_3 plasma (see Fig. 20, sequence I). We tested this potential SiC_xN_y ALD process using $SiCl_2(CH_3)_2$ as precursor, but no measurable C was incorporated into the growing film for two reasons. First, *in situ* ATR-FTIR spectroscopy showed that surface —CH_3 species were not present following the $SiCl_2(CH_3)_2$ reaction with an H-terminated SiN_x surface suggesting that —CH_3 is the leaving group during $SiCl_2(CH_3)_2$ chemisorption. Second, any —CH_3 species left after $SiCl_2(CH_3)_2$ chemisorption are likely to be abstracted in the subsequent NH_3 plasma step due to the presence of atomic H in the plasma. In the second tested approach, an SiC_xN_y film would be grown using a three-step ALD process where Si and C are brought to the surface using two reactive precursor exposure steps followed by an N_2 or NH_3 plasma step. We tested the feasibility of two ALD processes for this approach, one where the a silane-derived precursor, such as DSBAS could be combined with CH_3I and an NH_3/Ar or N_2/Ar plasma [see Fig. 20, sequence II(a)], and another where we tested an ALD processes using Si_2Cl_6, $Al(CH_3)_3$, and an NH_3/Ar or N_2/Ar plasma [see Fig. 20, sequence II(b)]. In the approach shown in Fig. 20, sequence II(a), we showed that while the CH_3I did react with a —SiH_x ($x = 1, 2, 3$) surface species that would be created by DSBAS chemisorption, the reaction did not result in —CH_x ($x = 1, 2, 3$) surface species most likely due to the formation of a —SiI_x ($x = 1, 2, 3$) with CH_4 as the reaction product.[48] In the approach shown in Fig. 20, sequence II(b), we show that $Al(CH_3)_3$ reacts with the —$SiCl_x$ ($x = 1, 2, 3$) terminated surface to form —$AlCH_3$ and —$SiCH_3$ surface species. However, the formation of —$AlCH_3$ surface species suggests that Al would be incorporated into the film. For the third approach, we attempted to a grow an SiC_xO_y film using a two-step ALD process that consisted of Si_2Cl_6 and an O_2/CO plasma [see Fig. 20, sequence III(a)]. However, when we tested this ALD process, either there was no C incorporated into the deposited SiO_2 film, or an amorphous carbon film was continuously deposited in the plasma cycle depending on the O_2 to CO ratio.

In a recent publication, using the C-containing plasma approach identified in Fig. 20, sequence III(b), we were able to successfully deposit a highly-conformal SiC_xN_y film at 400 °C using an ALD process that consisted of alternating exposures of Si_2Cl_6 and CH_3NH_2 plasma. We showed using dynamic SIMS depth profiling that a CH_3NH_2 plasma can be used to grow SiC_xN_y films with ~9% C (see Fig. 21) in a self-limiting manner. While the C content could be further increased to ~13% as the plasma power was increased from 100 to 200 W, the CH_3NH_2 plasma step was no longer self-limiting and led to continuous carbon nitride film growth, suggesting that the processing window in which a CH_3NH_2 plasma leads to self-limiting film growth is relatively narrow.

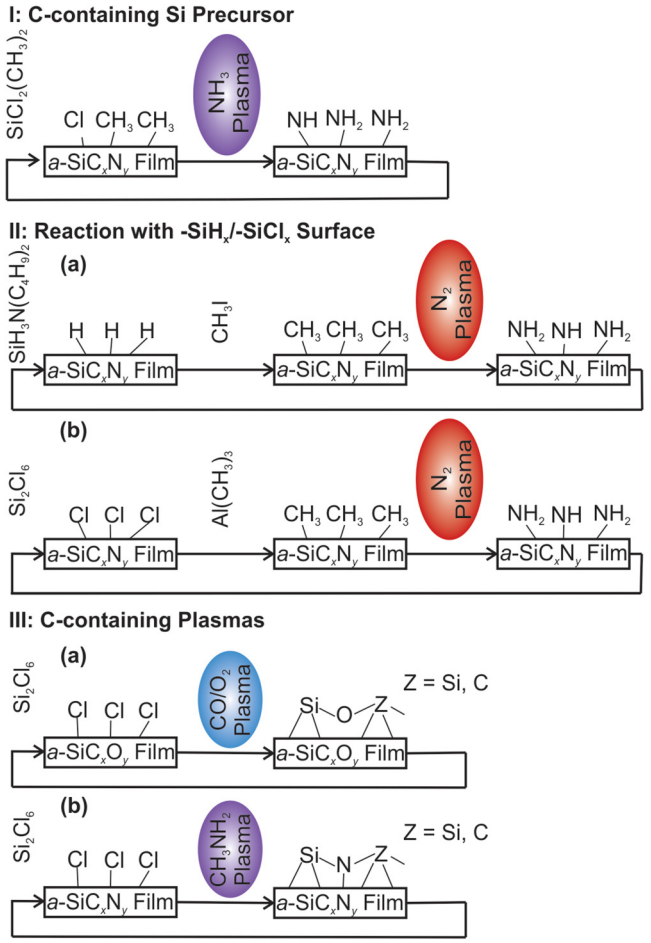

FIG. 20. Proposed ALD methods for the incorporation of C into SiN_x and SiO_2.

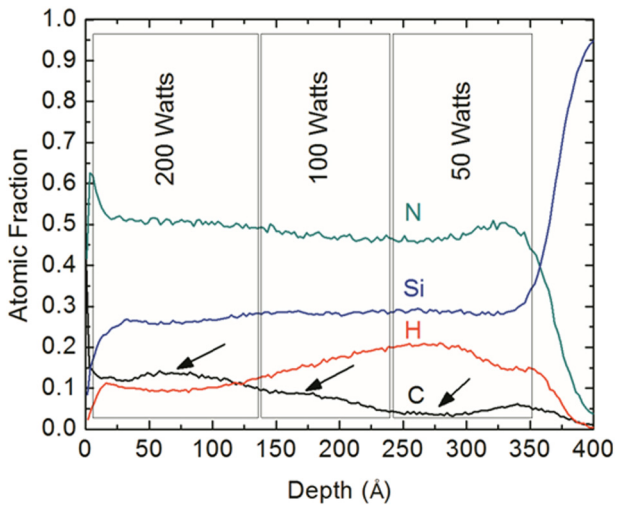

FIG. 21. Depth profile obtained using dynamic SIMS analysis of an SiC_xN_y stack deposited at 50, 100, and 200 W rf power to the CH_3NH_2 plasma. The arrows indicate the point at which the C-content was assumed to be at steady state. A depth of zero corresponds to the film surface. The Si wafer and film interface is at a depth of approximately 350 Å. Reprinted with permission from Ovanesyan *et al.*, Chem. Mater. **29**, 6269 (2017) (Ref. 49). Copyright 2017 American Chemical Society.

It was also found that the C was incorporated in the form of Si—N═C═N—Si species rather than as an Si—C—Si species, meaning that a true SiC phase is not actually present within the deposited SiC_xN_y film.

Recently, Lee and co-workers reported ALD of SiCO film with C-containing Si precursors.[178] These films deposited using octamethylcyclotetrasiloxane combined with either an H_2 or Ar plasma, contained between 20%–15% C and 11%–6% C, respectively. The films deposited using this approach exhibited dielectric constants that were lower than that of bulk SiO_2. Lee reported that using an O_2 plasma resulted in films that contained no measureable C,[178] a result similar to what we reported in a previous publication.[48]

Wang *et al.* tested a variety of C-containing aminosilane precursors with O_3 in an attempt to deposit SiCO films.[179] Wang and co-workers showed that using di-isopropylaminomethylsilane allows for the growth of SiCO films with a conformality of >95% and a C content of up to 8% at a substrate temperature of 100 °C. Wang showed that at higher substrate temperatures the C content of the films, irrespective of the aminosilane precursor, was reduced significantly.

To deposit SiCO using a different approach, Closser and co-workers used molecular layer deposition (MLD)—a thin film deposition technique similar to ALD.[180] MLD uses either homo- or hetero-bifunctional reactants for the deposition of organic and hybrid organic-inorganic materials. Closser *et al.* showed that using a bridged homo-bifunctional precursor, bis(trichlorosilyl)methane, and H_2O allows for the deposition of SiCO films at room temperature with a C content as high as 16.4%. The SiCO films had a dielectric constant of 2.6 ± 0.3, lower than that of bulk SiO_2, which is a desirable property for certain semiconductor manufacturing applications. As a technique for the deposition of C-containing Si-based dielectrics, MLD has shown promise, and could potentially enable the deposition of films with the properties necessary for integration into semiconductor manufacturing.[181,182]

The numerous challenges associated with the ALD of pure SiC, as well as the difficulties in incorporation of C into SiO_2 and Si_3N_4 films means that scientific breakthroughs are needed to enable the ALD of SiC, SiCN, and SiCO. These scientific breakthroughs could include substantially more reactive Si precursors and C precursors, novel C-containing plasmas that do not lead to *a*-C film growth and incorporate C in the proper bonding configuration, or new processes that take advantage of plasma activation or thermal annealing steps.

V. CONCLUSIONS

In this focused review, we have discussed the status of thermal and plasma-assisted ALD of the three Si-based dielectric films most relevant to the semiconductor industry: SiO_2, SiN_x, and SiC. We have also identified, whenever possible, the surface reaction mechanisms that lead to film growth and the effects that the reaction mechanisms have on bulk film properties. Our review of the literature shows that for the ALD of SiO_2, there are numerous thermal and plasma-assisted processes that can grow highly-conformal, device-quality SiO_2 films at a low temperature. We also describe the surface reaction mechanisms for thermal and plasma-assisted ALD processes for SiO_2, which are reasonably well understood. As plasma-assisted ALD of SiO_2 is already integrated in semiconductor manufacturing, the optimization of SiO_2 ALD processes—whether by improving the GPC, defect reduction, or via a decrease in the necessary precursor dose—is the primary focus of current process development. In contrast, while both thermal and plasma-assisted SiN_x ALD processes do exist, several processing challenges remain. For thermal SiN_x ALD processes, the two primary challenges are deposition temperatures that are typically >400 °C, and large N precursor doses, both of which are related to the inadequate reactivity of current N precursors. On the other hand, plasma-assisted SiN_x ALD processes typically suffer from either anisotropic film properties or low conformality for NH_3- and N_2-plasma-based ALD processes, respectively. Therefore, the future outlook for SiN_x ALD is the improvement and fine-tuning of current processes, whether by the use of more reactive precursors to improve film quality or by modification of the plasma step to enhance either the conformality or the film properties. Finally, in the case of SiC, no self-limiting low-temperature ALD processes exist. Therefore, the implementation of ALD of SiC in semiconductor manufacturing will require scientific breakthroughs in the development of new precursors and the use of new plasma chemistries.

ACKNOWLEDGMENTS

The authors would like to thank the Lam Research Corporation and the Lam Research Foundation for funding this work.

[1]J. A. Carballo, W. T. J. Chan, P. A. Gargini, A. B. Kahng and S. Nath, paper presented at the 2014 IEEE 32nd International Conference on Computer Design (ICCD), Seoul, 19 October 2014 (unpublished).
[2]C. Martin, Nat. Nanotechnol. **11**, 112 (2016).
[3]R. W. Johnson, A. Hultqvist, and S. F. Bent, Mater. Today **17**, 236 (2014).
[4]J. G. E. Gardeniers, H. A. C. Tilmans, and C. C. G. Visser, J. Vac. Sci. Technol. A **14**, 2879 (1996).
[5]D. Teasdale, Y. Senzaki, R. Herring, G. Hoeye, L. Page, and P. Schubert, Electrochem. Solid State Lett. **4**, F11 (2001).
[6]C. A. Murray, S. D. Elliott, D. Hausmann, J. Henri, and A. LaVoie, ACS Appl. Mater. Interfaces **6**, 10534 (2014).
[7]D. Dergez, J. Schalko, A. Bittner, and U. Schmid, Appl. Surf. Sci. **284**, 348 (2013).
[8]Y. B. Park and S. W. Rhee, J. Mater. Sci. Mater. Electron. **12**, 515 (2001).
[9]H. Lin, L. Q. Xu, X. Chen, X. H. Wang, M. Sheng, F. Stubhan, K. H. Merkel, and J. Wilde, Thin Solid Films **333**, 71 (1998).
[10]F. Koehler, D. H. Triyoso, I. Hussain, S. Mutas, and H. Bernhardt, *IOP, E-MRS 2012 Spring Meeting,* IOP, Strasbourg (May 14–18, 2012), Vol. 41, p. 012006.
[11]F. Koehler, D. H. Triyoso, I. Hussain, B. Antonioli, and K. Hempel, Phys. Status Solidi C **11**, 73 (2014).
[12]S. M. George, Chem. Rev. **110**, 111 (2010).
[13]H. B. Profijt, S. E. Potts, M. C. M. van de Sanden, and W. M. M. Kessels, J. Vac. Sci. Technol. A **29**, 050801 (2011).
[14]X. Meng, Y. C. Byun, H. S. Kim, J. S. Lee, A. T. Lucero, L. X. Cheng, and J. Kim, Materials **9**, 1007 (2016).

[15]V. Miikkulainen, M. Leskela, M. Ritala, and R. L. Puurunen, J. Appl. Phys. **113**, 021301 (2013).
[16]R. L. Puurunen, J. Appl. Phys. **97**, 121301 (2005).
[17]H. Van Bui, F. Grillo, and J. R. van Ommen, Chem. Commun. **53**, 45 (2017).
[18]E. Ahvenniemi *et al.*, J. Vac. Sci. Technol. A **35**, 010801 (2017).
[19]H. Kim, J. Vac. Sci. Technol. B **21**, 2231 (2003).
[20]D. M. Hausmann, E. Kim, J. Becker, and R. G. Gordon, Chem. Mater. **14**, 4350 (2002).
[21]N. Chandrasekaran, paper presented at the 2013 IEEE International Electron Devices Meeting, Washington, DC, 9–11 December 2013 (unpublished).
[22]A. E. Kaloyeros, F. A. Jové, J. Goff, and B. Arkles, ECS J. Solid State Sci. Technol. **6**, P691 (2017).
[23]J. S. Ponraj, G. Attolini, and M. Bosi, Crit. Rev. Solid State Mater. Sci. **38**, 203 (2013).
[24]D. Hausmann, J. Henri, J. Sims, K. Kelchner, S. Janjam, and S. Tang, *Meeting Abstracts MA2014-02*, ECS, Cancun Mexico (October 7 2014), p. 1608.
[25]R. J. Gasvoda, A. W. van de Steeg, R. Bhowmick, E. A. Hudson, and S. Agarwal, ACS Appl. Mater. Interfaces **9**, 31067 (2017).
[26]M. Belyansky *et al.*, in *Silicon Compatible Materials, Processes, and Technologies for Advanced Integrated Circuits and Emerging Applications 4*, edited by F. Roozeboom, K. Kakushima, E. P. Gusev, O. M. Leonte, V. Narayanan, P. J. Timans, and P. A. Kohl (ECS, Toronto, Canada, 2014), Vol. 61, p. 39.
[27]B. Yu *et al.*, paper presented at the 2015 China Semiconductor Technology International Conference, Shanghai, 15–16 March 2015 (unpublished).
[28]D. H. Triyoso *et al.*, ECS J. Solid State Sci. Technol. **2**, N222 (2013).
[29]A. B. Sachid, Y. M. Huang, Y. J. Chen, C. C. Chen, D. D. Lu, M. C. Chen, and C. Hu, IEEE Electron Device Lett. **38**, 16 (2017).
[30]M. R. Baklanov, M. V. Hove, G. Mannaert, S. Vanhaelemeersch, H. Bender, T. Conard, and K. Maex, J. Vac. Sci. Technol. B **18**, 1281 (2000).
[31]K. Maex, M. R. Baklanov, D. Shamiryan, F. Iacopi, S. H. Brongersma, and Z. S. Yanovitskaya, J. Appl. Phys. **93**, 8793 (2003).
[32]S. W. King, M. French, J. Bielefeld, and W. A. Lanford, J. Non-Cryst. Solids **357**, 2970 (2011).
[33]S. W. King, ECS J. Solid State Sci. Technol. **4**, N3029 (2015).
[34]H. C. Tsai, Y. S. Chang, and S. Y. Chang, Microelectron. Eng. **85**, 1658 (2008).
[35]P. Schiavone, C. Esclope and A. Halimaoui, 1999 (unpublished).
[36]P. Xu *et al.*, paper presented at the Proceedings of the SPIE, San Jose, California, 2011 (unpublished).
[37]X. Fu, G. Jian, J. Zhou, R. Jakkaraju, N. Yoshida and P. Ma, paper presented at the 2016 China Semiconductor Technology International Conference (CSTIC), Shanghai, China, 12–13 March 2016 (unpublished).
[38]J. Beynet *et al.*, paper presented at the SPIE Lithography Asia, Taipei, Taiwan, 18–19 November 2009 (unpublished).
[39]A. B. Kahng, C. H. Park, X. Xu, and H. Yao, IEEE T. Comput. Aid. D. **29**, 939 (2010).
[40]J. Park *et al.*, paper presented at the SPIE Photomask Technology, Monterey, CA, 18–22 September, 2006 (unpublished).
[41]K. Nakayama, C. Kodama, T. Kotani, S. Nojima, S. Mimotogi and S. Miyamoto, paper presented at the SPIE Advanced Lithography, San Jose, CA, 12–16 February, 2012 (unpublished).
[42]H. Singh, *Solid State Technology* (Extension Media, 2017), p. 18.
[43]K. Endo, Y. Ishikawa, T. Matsukawa, Y. Liu, O. Shin-ichi, K. Sakamoto, J. Tsukada, H. Yamauchi, and M. Masahara, Solid-State Electron. **74**, 13 (2012).
[44]S. D. Elliott, Semicond. Sci. Technol. **27**, 074008 (2012).
[45]R. P. Chaukulkar, N. F. W. Thissen, V. R. Rai, and S. Agarwal, J. Vac. Sci. Technol. A **32**, 01A108 (2013).
[46]R. P. Chaukulkar and S. Agarwal, J. Vac. Sci. Technol. A **31**, 031509 (2013).
[47]R. A. Ovanesyan, D. M. Hausmann, and S. Agarwal, ACS Appl. Mater. Interfaces **7**, 10806 (2015).
[48]R. A. Ovanesyan, D. M. Hausmann, and S. Agarwal, J. Vac. Sci. Technol. A **35**, 021506 (2017).
[49]R. A. Ovanesyan, N. Leick, K. M. Kelchner, D. M. Hausmann, and S. Agarwal, Chem. Mater. **29**, 6269 (2017).
[50]V. R. Rai and S. Agarwal, J. Phys. Chem. C **112**, 9552 (2008).
[51]V. R. Rai and S. Agarwal, J. Phys. Chem. C **113**, 12962 (2009).
[52]V. R. Rai and S. Agarwal, Chem. Mater. **23**, 2312 (2011).
[53]V. R. Rai and S. Agarwal, J. Vac. Sci. Technol. A **30**, 01A158 (2012).
[54]V. R. Rai, V. Vandalon, and S. Agarwal, Langmuir **26**, 13732 (2010).
[55]V. R. Rai, V. Vandalon, and S. Agarwal, Langmuir **28**, 350 (2012).
[56]N. Leick, R. O. F. Verkuijlen, L. Lamagna, E. Langereis, S. Rushworth, F. Roozeboom, M. C. M. van de Sanden, and W. M. M. Kessels, J. Vac. Sci. Technol. A **29**, 0210161 (2011).
[57]N. Leick, S. Agarwal, A. J. M. Mackus, S. E. Potts, and W. M. M. Kessels, J. Phys. Chem. C **117**, 21320 (2013).
[58]W. Cabrera, M. D. Halls, I. M. Povey, and Y. J. Chabal, J. Phys. Chem. C **118**, 29164 (2014).
[59]V. Vandalon and W. M. M. Kessels, J. Vac. Sci. Technol. A **35**, 05C313 (2017).
[60]H. C. M. Knoops, K. de Peuter, and W. M. M. Kessels, Appl. Phys. Lett. **107**, 014102 (2015).
[61]S. Weeks, G. Nowling, N. Fuchigami, M. Bowes, and K. Littau, J. Vac. Sci. Technol. A **34**, 01A140 (2016).
[62]T. Faraz, M. van Drunen, H. C. M. Knoops, A. Mallikarjunan, I. Buchanan, D. M. Hausmann, J. Henri, and W. M. M. Kessels, ACS Appl. Mater. Interfaces **9**, 1858 (2017).
[63]B. B. Burton, S. W. Kang, S. W. Rhee, and S. M. George, J. Phys. Chem. C **113**, 8249 (2009).
[64]Y. J. Chabal, Surf. Sci. Rep. **8**, 211 (1988).
[65]Y. J. Chabal, G. S. Higashi, K. Raghavachari, and V. A. Burrows, J. Vac. Sci. Technol. A **7**, 2104 (1989).
[66]E. A. Filatova, D. Hausmann, and S. D. Elliott, J. Vac. Sci. Technol. A **35**, 01B103 (2017).
[67]M. Shirazi and S. D. Elliott, J. Comput. Chem. **35**, 244 (2014).
[68]G. Fang, L. Xu, J. Ma, and A. Li, Chem. Mater. **28**, 1247 (2016).
[69]Y.-C. Jeong, S.-B. Baek, D.-H. Kim, J.-S. Kim, and Y.-C. Kim, Appl. Surf. Sci. **280**, 207 (2013).
[70]O. Sneh, M. L. Wise, A. W. Ott, L. A. Okada, and S. M. George, Surf. Sci. **334**, 135 (1995).
[71]C. P. Tripp and M. L. Hair, J. Phys. Chem. **97**, 5693 (1993).
[72]C. P. Tripp and M. L. Hair, Langmuir **8**, 1120 (1992).
[73]C. P. Tripp and M. L. Hair, Langmuir **8**, 1961 (1992).
[74]K. K. Unger, O. Jilge, J. N. Kinkel, and M. T. W. Hearn, J. Chromatogr. A **359**, 61 (1986).
[75]J. K. Kang and C. B. Musgrave, J. Appl. Phys. **91**, 3408 (2002).
[76]G. Y. Fang, L. N. Xu, L. G. Wang, Y. Q. Cao, D. Wu, and A. D. Li, Nanoscale Res. Lett. **10**, 68 (2015).
[77]J. P. Blitz, R. S. Shreedhara Murthy, and D. E. Leyden, J. Colloid Interface Sci. **126**, 387 (1988).
[78]J. W. Klaus, O. Sneh, and S. M. George, Science **278**, 1934 (1997).
[79]S. Chen, G. Fang, X. Qian, A. Li, and J. Ma, J. Phys. Chem. C **115**, 23363 (2011).
[80]Y. Su, X. Du and S, and M. George, J. Phys. Chem. C **111**, 219 (2007).
[81]J. W. Klaus and S. M. George, Surf. Sci. **447**, 81 (2000).
[82]S.-W. Lee, K. Park, B. Han, S.-H. Son, S.-K. Rha, C.-O. Park, and W.-J. Lee, Electrochem. Solid State Lett. **11**, G23 (2008).
[83]W. J. Lee, C. H. Han, J. K. Park, Y. S. Lee, and S. K. Rha, Jpn. J. Appl. Phys **49**, 071504 (2010).
[84]S. D. Elliott, G. Scarel, C. Wiemer, M. Fanciulli, and G. Pavia, Chem. Mater. **18**, 3764 (2006).
[85]J. D. Ferguson, E. R. Smith, A. W. Weimer, and S. M. George, J. Electrochem. Soc. **151**, G528–G535 (2004).
[86]J. Bachmann *et al.*, Angew. Chem. Int. Ed. Engl. **47**, 6177 (2008).
[87]L. Ju and N. C. Strandwitz, J. Mater. Chem. C **4**, 4034 (2016).
[88]D. Hausmann, J. Becker, S. Wang, and R. G. Gordon, Science **298**, 402 (2002).
[89]G. Ni, B. Han, and H. Cheng, J. Phys. Chem. C **117**, 22705 (2013).
[90]Y. Lu, A. Kobayashi, H. Kondo, K. Ishikawa, M. Sekine, and M. Hori, Jpn. J. Appl. Phys. **53**, 010305 (2014).
[91]L. F. Peña, C. E. Nanayakkara, A. Mallikarjunan, H. Chandra, M. Xiao, X. Lei, R. M. Pearlstein, A. Derecskei-Kovacs, and Y. J. Chabal, J. Phys. Chem. C **120**, 10927 (2016).
[92]S.-B. Baek, D.-H. Kim, and Y.-C. Kim, Appl. Surf. Sci. **258**, 6341 (2012).
[93]B. Han *et al.*, J. Phys. Chem. C **116**, 947 (2012).
[94]L. Huang *et al.*, J. Phys. Chem. C **117**, 19454 (2013).
[95]G. Y. Fang, L. N. Xu, Y. Q. Cao, L. G. Wang, D. Wu, and A. D. Li, Chem. Commun. **51**, 1341 (2015).

[96]J. Li, J. Wu, C. Zhou, B. Han, E. J. Karwacki, M. Xiao, X. Lei, and H. Cheng, J. Phys. Chem. C **113**, 9731 (2009).
[97]Y. Kinoshita, F. Hirose, H. Miya, K. Hirahara, Y. Kimura, and M. Niwano, Electrochem. Solid State Lett. **10**, G80 (2007).
[98]F. Hirose, Y. Kinoshita, S. Shibuya, Y. Narita, Y. Takahashi, H. Miya, K. Hirahara, Y. Kimura, and M. Niwano, Thin Solid Films **519**, 270 (2010).
[99]A. Mallikarjunan, H. Chandra, M. Xiao, X. Lei, R. M. Pearlstein, H. R. Bowen, M. L. O'Neill, A. Derecskei-Kovacs, and B. Han, J. Vac. Sci. Technol. A **33**, 01A137 (2015).
[100]G. Lucovsky, Solid State Commun. **29**, 571 (1979).
[101]C. C. Cheng *et al.*, Thin Solid Films **225**, 196 (1993).
[102]J.-M. Park, S. J. Jang, L. L. Yusup, W.-J. Lee, and S.-I. Lee, ACS Appl. Mater. Interfaces **8**, 20865 (2016).
[103]A. Nakajima, Q. D. M. Khosru, T. Yoshimoto, T. Kasai, and S. Yokoyama, Appl. Phys. Lett. **83**, 335 (2003).
[104]A. Nakajima, T. Yoshimoto, T. Kidera, and S. Yokoyama, Appl. Phys. Lett. **79**, 665 (2001).
[105]W. J. Lee, U. J. Kim, C. H. Han, M. H. Chun, and S. K. Rha, J. Korean Phys. Soc. **47**, S598 (2005).
[106]W. J. Lee, J. H. Lee, C. O. Park, Y. S. Lee, S. J. Shin, and S. K. Rha, J. Korean Phys. Soc. **45**, 1352 (2004).
[107]J. W. Klaus, A. W. Ott, A. C. Dillon, and S. M. George, Surf. Sci. **418**, L14 (1998).
[108]A. Nakajima, T. Yoshimoto, T. Kidera, K. Obata, S. Yokoyama, H. Sunami, and M. Hirose, Appl. Phys. Lett. **77**, 2855 (2000).
[109]A. Nakajima, T. Yoshimoto, T. Kidera, K. Obata, S. Yokoyama, H. Sunami, and M. Hirose, J. Vac. Sci. Technol. B **19**, 1138 (2001).
[110]Q. D. M. Khosru, A. Nakajima, T. Yoshimoto, and S. Yokoyama, Appl. Phys. Lett. **79**, 3488 (2001).
[111]A. Nakajima, Q. D. M. Khosru, T. Yoshimoto, and S. Yokoyama, Mictroelectron. Reliab. **42**, 1823 (2002).
[112]A. Nakajima, Q. D. M. Khosru, T. Yoshimoto, T. Kidera, and S. Yokoyama, Appl. Phys. Lett. **80**, 1252 (2002).
[113]A. Nakajima, Q. D. M. Khosru, T. Yoshimoto, T. Kidera, and S. Yokoyama, J. Vac. Sci. Technol. B **20**, 1406 (2002).
[114]S. Zhu and A. Nakajima, Jpn. J. Appl. Phys. **46**, 7699 (2007).
[115]W. Hansch, A. Nakajima, and S. Yokoyama, Appl. Phys. Lett. **75**, 1535 (1999).
[116]K. Park, W.-D. Yun, B.-J. Choi, H.-D. Kim, W.-J. Lee, S.-K. Rha, and C. O. Park, Thin Solid Films **517**, 3975 (2009).
[117]L. L. Yusup, J.-M. Park, Y.-H. Noh, S.-J. Kim, W.-J. Lee, S. Park, and Y.-K. Kwon, RSC Adv. **6**, 68515 (2016).
[118]S. Morishita, S. Sugahara, and M. Matsumura, Appl. Surf. Sci. **112**, 198 (1997).
[119]M. Edmonds *et al.*, J. Chem. Phys. **146**, 052820 (2017).
[120]S. Riedel, J. Sundqvist, and T. Gumprecht, Thin Solid Films **577**, 114 (2015).
[121]S. Yokoyama, H. Goto, T. Miyamoto, N. Ikeda, and K. Shibahara, Appl. Surf. Sci. **112**, 75 (1997).
[122]H. Goto, K. Shibahara, and S. Yokoyama, Appl. Phys. Lett. **68**, 3257 (1996).
[123]S. Yokoyama, N. Ikeda, K. Kajikawa, and Y. Nakashima, Appl. Surf. Sci. **130**, 352 (1998).
[124]K. Nagata, M. Nagasaka, T. Yamaguchi, A. Ogura, H. Oji, J.-Y. Son, I. Hirosawa, Y. Watanabe, and Y. Hirota, ECS Trans. **53**, 51 (2013).
[125]J. Provine, P. Schindler, Y. Kim, S. P. Walch, H. J. Kim, K.-H. Kim, and F. B. Prinz, AIP Adv. **6**, 065012 (2016).
[126]T. Iwao, P. L. G. Ventzek, R. Upadhyay, L. L. Raja, H. Ueda, and K. Ishibashi, J. Vac. Sci. Technol. A **36**, 01A111 (2018).
[127]H. S. Kim *et al.*, ACS Appl. Mater. Interfaces **10**, 44825 (2018).
[128]R. H. E. C. Bosch, L. E. Cornelissen, H. C. M. Knoops, and W. M. M. Kessels, Chem. Mater. **28**, 5864 (2016).
[129]H. C. M. Knoops, E. M. J. Braeken, K. de Peuter, S. E. Potts, S. Haukka, V. Pore, and W. M. M. Kessels, ACS Appl. Mater. Interfaces **7**, 19857 (2015).
[130]A. M. Andringa, A. Perrotta, K. de Peuter, H. C. M. Knoops, W. M. M. Kessels, and M. Creatore, ACS Appl. Mater. Interfaces **7**, 22525 (2015).
[131]Y. Kim *et al.*, ACS Appl. Mater. Interfaces **8**, 17599 (2016).
[132]N. Leick, J. M. M. Huijs, R. A. Ovanesyan, D. M. Hausmann and S. Agarwal, Plasma Process. Polym. **16**, 1900032 (2019).
[133]S. Suh, S. W. Ryu, S. Cho, J.-R. Kim, S. Kim, C. S. Hwang, and H. J. Kim, J. Vac. Sci. Technol. A **34**, 01A136 (2016).
[134]J.-H. Han, J.-M. Choi, S.-H. Lee, W. Jeon, and J.-S. Park, Ceram. Int. **44**, 20890 (2018).
[135]J.-M. Park, S. J. Jang, S.-I. Lee, and W.-J. Lee, ACS Appl. Mater. Interfaces **10**, 9155 (2018).
[136]W. Jang, H. Jeon, C. Kang, H. Song, J. Park, H. Kim, H. Seo, M. Leskela, and H. Jeon, Phys. Status Solidi A **211**, 2166 (2014).
[137]W. Jang, H. Jeon, H. Song, H. Kim, and J. Park, Phys. Status Solidi A **212**, 2785 (2015).
[138]W. Jang *et al.*, J. Vac. Sci. Technol. A **36**, 031514 (2018).
[139]S. W. King, J. Vac. Sci. Technol. A **29**, 041501 (2011).
[140]S. King, ECS Trans. **33**, 365 (2010).
[141]J.-S. Park, S.-W. Kang, and H. Kim, J. Vac. Sci. Technol. B **24**, 1327 (2006).
[142]H. Kim, H. Song, C. Shin, K. Kim, W. Jang, H. Kim, S. Shin, and H. Jeon, J. Vac. Sci. Technol. A **35**, 01A101 (2017).
[143]S. Agarwal, A. Takano, M. C. M. van de Sanden, D. Maroudas, and E. S. Aydil, J. Chem. Phys. **117**, 10805 (2002).
[144]S. Sriraman, S. Agarwal, E. S. Aydil, and D. Maroudas, Nature **418**, 62 (2002).
[145]S. Agarwal, S. Sriraman, A. Takano, M. C. M. van de Sanden, E. S. Aydil, and D. Maroudas, Surf. Sci. **515**, L469 (2002).
[146]L. L. Yusup, J.-M. Park, T. R. Mayangsari, Y.-K. Kwon, and W.-J. Lee, Appl. Surf. Sci. **432**, 127 (2018).
[147]M. Dai, Y. Wang, J. Kwon, M. D. Halls, and Y. J. Chabal, Nat. Mater. **8**, 825 (2009).
[148]D. V. Tsu, G. Lucovsky, and M. J. Mantini, Phys. Rev. B **33**, 7069 (1986).
[149]S. Rivillon, F. Amy, Y. J. Chabal, and M. M. Frank, Appl. Phys. Lett. **85**, 2583 (2004).
[150]S. J. Kang and V. M. Donnelly, Plasma Sources Sci. Technol. **16**, 265 (2007).
[151]G. Hartmann, P. L. G. Ventzek, T. Iwao, K. Ishibashi, and G. S. Hwang, Phys. Chem. Chem. Phys. **20**, 29152 (2018).
[152]D. Hausmann, paper presented at the AVS 17th International Conference on Atomic Layer Deposition, Denver, CO, 15–18 July 2017 (unpublished).
[153]L. Huang *et al.*, Phys. Chem. Chem. Phys. **16**, 18501 (2014).
[154]G. Scardera, T. Puzzer, G. Conibeer, and M. A. Green, J. Appl. Phys. **104**, 104310 (2008).
[155]M. J. Kong, K. S. Lee, J. Lyubovitsky, and S. F. Bent, Chem. Phys. Lett. **263**, 1 (1996).
[156]L. F. Peña *et al.*, Langmuir **34**, 2619 (2018).
[157]C. K. Ande, H. C. M. Knoops, K. de Peuter, M. van Drunen, S. D. Elliott, and W. M. M. Kessels, J. Phys. Chem. Lett. **6**, 3610 (2015).
[158]E. A. Filatova, D. Hausmann, and S. D. Elliott, ACS Appl. Mater. Interfaces **10**, 15216 (2018).
[159]T. Fuyuki, T. Yoshinobu, and H. Matsunami, Thin Solid Films **225**, 225 (1993).
[160]T. Fuyuki, M. Nakayama, T. Yoshinobu, H. Shiomi, and H. Matsunami, J. Cryst. Growth **95**, 461 (1989).
[161]S. Hara, Y. Aoyagi, M. Kawai, S. Misawa, E. Sakuma, and S. Yoshida, Surf. Sci. **273**, 437 (1992).
[162]S. Hara, T. Meguro, Y. Aoyagi, M. Kawai, S. Misawa, E. Sakuma, and S. Yoshida, Thin Solid Films **225**, 240 (1993).
[163]J. J. Sumakeris, L. B. Rowland, R. S. Kern, S. Tanaka, and R. F. Davis, Thin Solid Films **225**, 219 (1993).
[164]H. Nagasawa and Y. Yamaguchi, Thin Solid Films **225**, 230 (1993).
[165]H. Nagasawa and Y. Yamaguchi, Appl. Surf. Sci. **82–83**, 405 (1994).
[166]E. Sadayuki, S. Imai, and M. Matsumura, Jpn. J. Appl. Phys. **34**, 6166 (1995).
[167]K. Yoshida, K. Matsumoto, T. Oguchi, K. Tonokura, and M. Koshi, J. Phys. Chem. A **110**, 4726 (2006).
[168]W. Beyer, Sol. Energ. Mat. Sol. Cells **78**, 235 (2003).
[169]J. L. Lin and B. E. Bent, J. Phys. Chem. **96**, 8529 (1992).
[170]A. P. Bento and F. M. Bickelhaupt, J. Org. Chem. **73**, 7290 (2008).
[171]H. Gutleben, S. R. Lucas, C. C. Cheng, W. J. Choyke, and J. T. Yates, Surf. Sci. **257**, 146 (1991).
[172]K. T. Wong and N. S. Lewis, Acc. Chem. Res. **47**, 3037 (2014).
[173]D. Kim, S.-H. Kim, and H. Kim, Mater. Sci. Semicond. Process. **29**, 139 (2015).
[174]K. M. Lee, C. Y. Kim, C. K. Choi, and R. Navamathavan, J. Korean Phys. Soc. **59**, 3074 (2011).

[175]C. Y. Kim, H. S. Lee, C. K. Choi, Y. H. Yu, R. Navamathavan, and H. J. Lee, J. Korean Phys. Soc. **62**, 1143 (2013).
[176]J. Zhang, D. S. Wavhal, and E. R. Fisher, J. Vac. Sci. Technol. A **22**, 201 (2004).
[177]M. J. Loboda, Microelectron. Eng. **50**, 15 (2000).
[178]J. Lee, W. Jang, H. Kim, S. Shin, Y. Kweon, K. Lee, and H. Jeon, Thin Solid Films **645**, 334 (2018).
[179]M. Wang, H. Chandra, X. Lei, A. Mallikarjunan, K. Cuthill, and M. Xiao, J. Vac. Sci. Technol. A **36**, 021509 (2018).
[180]R. G. Closser, D. S. Bergsman, and S. F. Bent, ACS Appl. Mater. Interfaces **10**, 24266 (2018).
[181]H. Zhou and S. F. Bent, J. Phys. Chem. C **117**, 19967 (2013).
[182]S. M. George, B. Yoon, and A. A. Dameron, Acc. Chem. Res. **42**, 498 (2009).